Small-signal Stability Criteria in Power Electronics-dominated Power Systems: A Comparative Review

Qifan Chen, *Graduate Student Member*, *IEEE*, Siqi Bu, *Senior Member*, *IEEE*, and Chi Yung Chung, *Fellow*, *IEEE*

***Abstract*—To tackle emerging power system small-signal stability problems such as wideband oscillations induced by the large-scale integration of renewable energy and power electronics, it is crucial to review and compare existing small-signal stability analysis methods. On this basis, guidance can be provided on determining suitable analysis methods to solve relevant small-signal stability problems in power electronics-dominated power systems (PEDPSs). Various mature methods have been developed to analyze the small-signal stability of PEDPSs, including eigenvalue-based methods, Routh stability criterion, Nyquist/Bode plot based methods, passivity-based methods, positive-net-damping method, lumped impedance-based methods, bifurcation-based methods, etc. In this paper, the application conditions, advantages, and limitations of these criteria in identifying oscillation frequencies and stability margins are reviewed and compared to reveal and explain connections and discrepancies among them. Especially, efforts are devoted to mathematically proving the equivalence between these small-signal stability criteria. Finally, the performance of these criteria is demonstrated and compared in a 4-machine 2-area power system with a wind farm and an IEEE 39-bus power system with 3 wind farms.**

***Index Terms*—Impedance-based method, oscillation analysis, power electronic converter, power electronics-dominated power system, renewable power generation, small-signal stability.**

I. Introduction

THE growth of renewable energy penetration is an inevitable trend in response to the carbon neutrality target. Growing renewable power generation via power electronic devices is foreseeable, which may introduce new wideband oscillation problems to modern power systems [1] - [4]. In power electronics-dominated power systems (PEDPSs), oscillations involve not only traditional synchronous generators (SGs) but also different control circuits of power electronic converters, e.g., phase locked loop and current loop control. Compared with the SG-induced oscillations, the power electronic converter-induced oscillations have very different mechanisms and present a wider oscillation frequency range, posing critical challenges for existing small-signal stability analysis.

In order to analyze the small-signal stability of PEDPSs, many small-signal stability criteria (SC) have been developed and successfully implemented, e.g., eigenvalue/pole based methods [5] - [17], Routh stability criterion [18] - [20], Nyquist/Bode plot based methods [21] - [30], passivity-based methods [31] - [35], positive-net-damping method [36] - [39], lumped impedance-based methods [40] - [42], bifurcation-based methods [43]-[46]. Based on these methods, the small-signal stability of a PEDPS can be analyzed in time domain [5] - [9], *s* domain (i. e., complex frequency domain) [15], [16], [18], [19], and frequency domain [21]-[24], [39]-[41], [47], [48]. The time-domain-based methods mainly include time-domain simulation and eigenvalue analysis based on accurate and detailed state-space models. A transfer function with respect to a complex argument, i.e., *s*, is used for the *s*-domain-based methods. The frequency-domain-based methods refer to the analysis of a transfer function with respect to a real argument, i. e., frequency. So-called impedance-based methods mainly employ the *s*-domain-based methods and the frequency-domain-based methods to analyze impedance-based transfer functions [7], [49]. Different limitations are encountered in PEDPSs due to the characteristics of these methods [23], [39], [50]. Specifically, some criteria may become inaccurate or infeasible under certain conditions. Massive power electronic converters pose a serious challenge in obtaining accurate models required by these methods. Furthermore, although these methods have seemingly different criteria for determining the frequencies and margins of oscillations, they are essentially linked. Therefore, to provide effective guidance on finding suitable analysis tools for emerging oscillation problems in PEDPSs, it is crucial to clearly reveal and explain the connections and discrepancies among different small-signal SC and the causes of their limitations. In [50], the impedance-based sufficient SC and Nyquist/Bode plot based methods are reviewed in a vehicle-grid system. In [23], a typical impedance-based method, Ny-

Manuscript received: August 8, 2023; revised: October 7, 2023; accepted: November 1, 2023. Date of CrossCheck: November 1, 2023. Date of online publication: December 12, 2023.

This work was supported in part by the National Natural Science Foundation of China for the Research Project (No. 52077188) and in part by the Hong Kong Research Grant Council for the Research Project (No. 15219619).

Q. Chen and C. Y. Chung are with Department of Electrical and Electronic Engineer, The Hong Kong Polytechnic University, Hong Kong, China (e-mail: qf_chen@foxmail.com; c.y.chung@polyu.edu.hk).

S. Bu (corresponding author) is with Department of Electrical and Electronic Engineering, Shenzhen Research Institute, Centre for Grid Modernisation, International Centre of Urban Energy Nexus, Centre for Advances in Reliability and Safety, Research Institute for Smart Energy, and Policy Research Centre for Innovation and Technology, The Hong Kong Polytechnic University, Hong Kong, China (e-mail: siqi.bu@polyu.edu.hk).

DOI: 10.35833/MPCE.2023.000526

quist/Bode plots, and eigenvalue analysis are compared in a weak grid with a voltage source converter. Six types of conservative impedance-based small-signal SC in DC power distribution systems are discussed in [51]. In existing literature, the connections between these criteria, especially some emerging methods (e. g., lumped impedance-based methods and positive-net-damping method), are rarely discussed. Moreover, the SC and the oscillation mode identification criteria (OMIC) of these methods are seldom investigated systematically or compared rigorously in a large-scale system.

Hence, eight types of small-signal stability analysis methods are reviewed and compared in this paper. The connections and discrepancies between different criteria are mathematically and thoroughly revealed. Meanwhile, the causes of the invalidation of these criteria under some conditions are explained.

The organization of this paper is as follows. Section II summarizes different small-signal models in a PEDPS. Section III details eight types of small-signal SC for PEDPSs in detail. Section IV compares different SC to analytically demonstrate their essential equivalence and discrepancies. Case studies are implemented in Section V to numerically compare the performance of different SC. Section VI discusses future challenges. Finally, conclusions are given in Section VII.

II. Small-signal Modeling for PEDPSs

Accurate small-signal stability analysis relies on an appropriate model of a power system. The increasing renewable power generation via power electronic devices raises a dynamic behavior different from that of a conventional power system dominated by SGs. A recent report in [52] summarizes the emerging stability phenomena induced by converters. It is indicated that the PEDPS exhibits a dynamic response that is more dependent on fast-response converters compared with the conventional power system dominated by SGs, resulting in emerging challenges regarding black-box modeling, high model dimension, wideband frequency characteristics, and new oscillation mechanisms. Specifically, the detailed structure and parameters of converters are kept usually confidential by manufacturers, and thus can hardly be modeled as white-box models. The number and order of converter models are obviously more than those of SGs, resulting in an extremely high-order system model. The frequency of power electronic switches or control loops can be from several to several thousand Hertz. Thus, small-signal stability problems in multiple time scales co-exist in the PEDPS, resulting in oscillations in a wide frequency range rather than only the conventional electromechanical low-frequency oscillations (LFOs). The mechanism of the emerging wideband oscillations is quite different from the conventional LFOs, requiring new and accurate models. These characteristics of PEDPS introduce tricky challenges for small-signal modeling and analysis. It is necessary to clarify appropriate models for analyzing the oscillatory phenomena in the PEDPS.

Converters have nonlinear and periodic behaviors.

1) A switching modulation process can be neglected or averaged over an appropriate period to eliminate the discontinuity. Then, a linear-time-invariant model can be derived in the *dq*-frame [8], [9]. The converter models in the *dq*-frame can be conveniently integrated with other *dq*-frame models of conventional components, e. g., SGs, for further analysis. It should be noted that the effects of three-phase unbalance and harmonics can hardly be analyzed based on the *dq*-frame model since the model would become time-varying [49], [53].

2) Considering the periodic time-varying features induced by three-phase unbalance and harmonics, harmonic linearization techniques, dynamic phasor (DP) techniques, and harmonic state-space (HSS) techniques can be employed. Harmonic linearization techniques enable linearizing a converter model at a time-varying operating point, and thus a sequence impedance model can be derived to analyze both balanced and unbalanced power systems as well as the effects of harmonics [53], [54]. The harmonic linearization involves lengthy algebra and thus a high computational cost for a system with massive converters. DP techniques [55], [56] and HSS techniques [49], [57] can also be employed for small-signal modeling considering any harmonics and frequency-coupling dynamics. The HSS techniques use linearization first and then Fourier series expansion to derive an HSS model. The DP techniques employ Fourier series expansion by generalized averaging operators first and then linearization to yield a linear-time-invariant model. The harmonic linearization, DP, and HSS techniques are valid for both balanced and unbalanced power systems, and thus are worthy of further study.

According to associated domains, these small-signal models can be divided into state-space models in time domain, transfer function models in *s* domain, and transfer functions in frequency domain. The *dq*-frame models can be described by state-space models in time domain and transfer functions in *s* domain or frequency domain. When considering periodic time-varying features induced by system unbalance and harmonics, the state-space models can be derived by DP and HSS techniques. The transfer function models in either *s* domain or frequency domain can be obtained by harmonic linearization techniques and the harmonic transfer function derived from an HSS.

The state-space model is a white-box model requiring a detailed knowledge of the power system. By contrast, the transfer function models are quite popular and considered promising for small-signal stability analysis in the PEDPS since they can be derived from a black-box representation of converters by measurement. The transfer function models in *s* and frequency domains can be conveniently modeled as impedance. Hence, the small-signal stability analysis in *s* and frequency domains is often collectively referred to as impedance-based analysis. However, an additional step of estimating techniques, e.g., vector fitting [58], [59], is necessary for deriving the *s*-domain model from measurements. Therefore, the frequency-domain-based modeling is easier to realize compared with the *s*-domain-based modeling.

Based on different types of models, various SC can be employed for small-signal stability analysis in the PEDPS, which is introduced in Section III.

III. Different Small-signal SC for PEDPSs

A. Eigenvalue

The eigenvalue-based methods, including modal analysis [6], [60] and damping torque analysis [61], [62], are well-known tools for the small-signal stability of traditional power systems, which have been successfully employed in PEDPSs with various power electronic devices, e.g., voltage source converter [23] and modular multilevel converter [30].

A PEDPS can be described by a set of differential-algebraic equations (DAEs) as:

$$\begin{cases} \dot{\boldsymbol{x}} = \boldsymbol{f}\left(\boldsymbol{x}, \boldsymbol{y}, \boldsymbol{p}_{\mathrm{s}}\right) \\ \boldsymbol{0} = \boldsymbol{g}\left(\boldsymbol{x}, \boldsymbol{y}, \boldsymbol{p}_{\mathrm{s}}\right) \end{cases} \tag{1}$$

where $\boldsymbol{x} \in \mathbb{R}^n$ is a dynamic variable vector; $\boldsymbol{y} \in \mathbb{R}^m$ is an algebraic variable vector; $\dot{\boldsymbol{x}} \in \mathbb{R}^n$ is the derivative of $\boldsymbol{x}$; $\boldsymbol{p}_{\mathrm{s}} \in \mathbb{R}^v$ is a parameter vector of the power system; and $\boldsymbol{f} \in \mathbb{R}^n$ and $\boldsymbol{g} \in \mathbb{R}^m$ are two groups of mapping functions.

For small-signal stability analysis, the dynamics of the variables of a PEDPS can be treated as almost linear. Thus, the DAEs can be linearized at a steady operating condition as [60], [61]:

$$\begin{cases} \Delta\dot{\boldsymbol{x}} = \tilde{\boldsymbol{A}}\Delta\boldsymbol{x} + \tilde{\boldsymbol{B}}\Delta\boldsymbol{y} \\ 0 = \tilde{\boldsymbol{C}}\Delta\boldsymbol{x} + \tilde{\boldsymbol{D}}\Delta\boldsymbol{y} \end{cases} \tag{2}$$

where Δ denotes a deviation operator; and $\tilde{\boldsymbol{A}} \in \mathbb{R}^{n\times n}$, $\tilde{\boldsymbol{B}} \in \mathbb{R}^{n\times m}$, $\tilde{\boldsymbol{C}} \in \mathbb{R}^{m\times n}$, and $\tilde{\boldsymbol{D}} \in \mathbb{R}^{m\times m}$ are the corresponding Jacobian matrices which are dependent on $\boldsymbol{p}_{\mathrm{s}}$.

By deleting $\Delta\boldsymbol{y}$ in (2), we can yield:

$$\Delta\dot{\boldsymbol{x}} = \boldsymbol{A}_{\mathrm{s}}\Delta\boldsymbol{x} \tag{3}$$

$\boldsymbol{A}_{\mathrm{s}} \in \mathbb{R}^{n\times n}$ can be derived by:

$$\boldsymbol{A}_{\mathrm{s}} = \tilde{\boldsymbol{A}} - \tilde{\boldsymbol{B}}\tilde{\boldsymbol{D}}^{-1}\tilde{\boldsymbol{C}} \tag{4}$$

In this paper, the small-signal SC for each method is summarized, and the OMIC is summarized if existing.

According to Lyapunov's first method, the small-signal stability can be analyzed using eigenvalues of $\boldsymbol{A}_{\mathrm{s}}$, as indicated by SC 1 [6].

SC 1: the whole power system is stable if the real part of all eigenvalues is negative; otherwise, the system is unstable.

The potential oscillation modes (OMs) can be obtained by OMIC 1 [6].

OMIC 1: each pair of conjugate eigenvalues $\sigma \pm \mathrm{j}\beta$, where j is an imaginary unit, corresponds to a specific OM. The oscillation frequency is $\beta/(2\pi)$ Hz. If $\sigma < 0$, the OM is stable; otherwise, the OM is unstable. The smaller σ is, the more stable the OM is.

In addition to state-space equations, the PEDPS can be described by transfer functions. A closed-loop transfer function (CLTF) $F(s)$ can be determined by (5), and the block diagram is shown in Fig. 1, where ΔW_{F} and ΔU_{F} are the input and output, respectively.

$$F(s) = \left(1 + G(s)H(s)\right)^{-1} G(s) \tag{5}$$

where s is a complex variable; $G(s)$ and $H(s)$ are the transfer functions of the forward and feedback paths, respectively; $G(s)H(s)$ is the open-loop transfer function (OLTF); and 1 will be replaced by an identity matrix $\boldsymbol{I}$ if $F(s)$ is a multiple-input multiple-output (MIMO) CLTF.

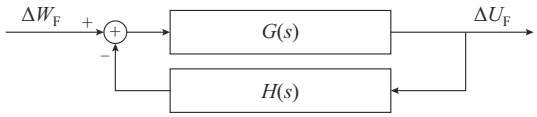

Fig. 1. Block diagram of a closed-loop PEDPS.

An open-loop subsystem corresponding to $G(s)$ or $H(s)$ individually can be described by a group of state-space equations as:

$$\begin{cases} \Delta\dot{\boldsymbol{X}} = \boldsymbol{A}\Delta\boldsymbol{X} + \boldsymbol{B}\Delta\boldsymbol{U} \\ \Delta\boldsymbol{W} = \boldsymbol{C}\Delta\boldsymbol{X} + \boldsymbol{D}\Delta\boldsymbol{U} \end{cases} \tag{6}$$

where $\boldsymbol{X}$ is a system state variable vector; $\dot{\boldsymbol{X}}$ is the derivative of $\boldsymbol{X}$; $\boldsymbol{U}$ is an input vector; $\boldsymbol{W}$ is an output vector; and $\boldsymbol{A}$, $\boldsymbol{B}$, $\boldsymbol{C}$, and $\boldsymbol{D}$ are the state-space matrices.

The state-space equations in (6) can be transformed to a state-space model in s domain by Laplace transformation. Then, the corresponding unique transfer function $G(s)$ or $H(s)$ can be derived by:

$$G(s) \text{ or } H(s) = \boldsymbol{C}\left(s\boldsymbol{I} - \boldsymbol{A}\right)^{-1}\boldsymbol{B} + \boldsymbol{D} \tag{7}$$

The pole set of the CLTF $F(s)$ is the subset of the eigenvalues of $\boldsymbol{A}_{\mathrm{s}}$. Specifically, the poles are completely equal to the eigenvalues if zero-pole cancellation (ZPC) does not exist [63]. Thus, SC 1 and OMIC 1 can be adopted to analyze the small-signal stability based on the poles of $F(s)$.

Concrete and accurate mathematical models are necessary for the application of eigenvalue-based methods. The analysis results are extremely reliable if the mathematical models are accurate enough. Thus, the results of eigenvalues and poles are usually adopted as a benchmark.

B. Routh Stability Criterion

The essence of calculating eigenvalues or poles is to solve the roots of an n^{th} order polynomial like:

$$P(s) = a_0 + a_1 s + a_2 s^2 + \ldots + a_n s^n \tag{8}$$

where $a_0, a_1, \ldots, a_n$ are the coefficients of the polynomial.

The polynomial is extremely high order for practical power system models, resulting in difficult solutions. Thus, the Routh stability criterion is proposed to determine the sign of the real part of eigenvalues or poles without solving the polynomial [18]. Customarily, making a_n positive, the power system is unstable if any coefficient in (8) is not positive. Otherwise, a Routh table as (9) can be listed for further analysis.

$$\begin{array}{ccc} a_n & a_{n-2} & \cdots \\ a_{n-1} & a_{n-3} & \cdots \\ b_1 & b_2 & \cdots \\ c_1 & c_2 & \cdots \\ \vdots & \vdots & \end{array} \tag{9}$$

$$b_i = -\frac{1}{a_{n-1}} \det\left(\begin{bmatrix} a_n & a_{n-2i} \\ a_{n-1} & a_{n-(2i+1)} \end{bmatrix}\right) \quad i = 1, 2, \ldots \tag{10}$$

$$c_i = -\frac{1}{b_1} \det\left(\begin{bmatrix} a_{n-1} & a_{n-(2i+1)} \\ b_1 & b_{i+1} \end{bmatrix}\right) \quad i = 1, 2, \ldots \tag{11}$$

The elements in (9) are calculated row by row from top to bottom until all remaining elements to be calculated are zeros. The number of eigenvalues with non-negative real parts is the number of sign changes of the elements in the first column of (9). Then, the small-signal stability can be judged by SC 2.

SC 2: the whole power system is stable if all coefficients in (8) are positive and the sign of the elements in the first column of (9) is positive; otherwise, the system is unstable.

The cornerstone of the Routh stability criterion is SC 1. However, the frequency of oscillations cannot be identified by the Routh stability criterion.

C. Nyquist Plot Based Methods

The above eigenvalue-based methods rely on the state-space models or CLTFs in s domain. By contrast, Nyquist plots can be employed to analyze the small-signal stability for a closed-loop power system only based on the frequency response of an OLTF. The Nyquist plot based methods have been widely implemented to analyze the small-signal stability in PEDPSs [50], [64].

Define an OLTF as:

$$L(s)=G(s)H(s) \tag{12}$$

By replacing s of $L(s)$ with jω, a Nyquist plot can be derived, where $\omega\in(-\infty,+\infty)$ is an angular frequency variable. Draw the locus of $L(\mathrm{j}\omega)$ in a complex plane, as shown in Fig. 2(a).

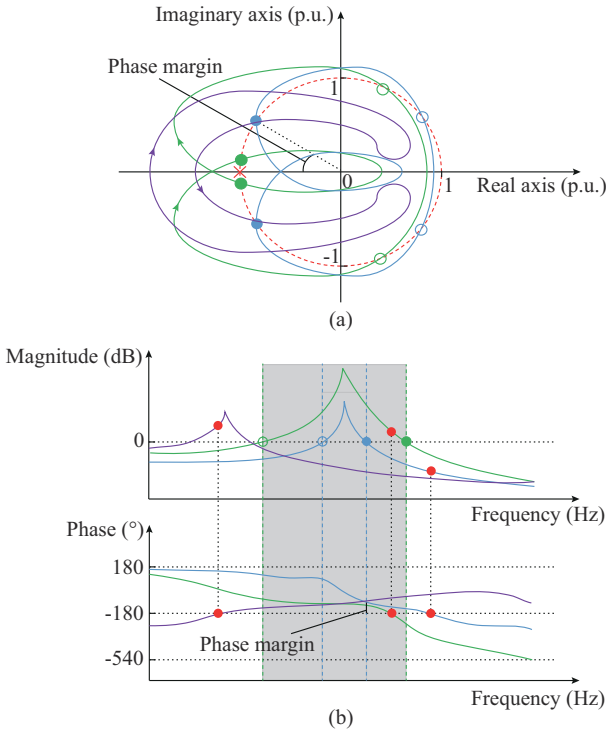

Fig. 2. Nyquist/Bode plots of $L(\mathrm{j}\omega)$ for stable or unstable power systems. (a) Nyquist plots. (b) Bode plots.

The encirclements in Nyquist plots satisfy:

$$N_{\mathrm{p,c}}=N_{\mathrm{p,o}}-N_{\mathrm{r}} \tag{13}$$

where $N_{\mathrm{p,c}}$ is the number of the poles of the CLTF $F(s)$ in the right-half plane (RHP); $N_{\mathrm{p,o}}$ is the number of the poles of $L(\mathrm{j}\omega)$ in the RHP; and N_{r} is the number of anticlockwise encirclements around point $(-1,\mathrm{j}0)$ in $L(\mathrm{j}\omega)$ locus.

According to SC 1, the small-signal stability can be judged by whether the poles of $F(s)$ exist in the RHP. Therefore, the Nyquist stability criterion is given as follows.

SC 3A: the closed-loop power system is stable when $N_{\mathrm{p,c}}=0$; otherwise, the system is unstable.

In practice, the open-loop subsystems usually are designed to be independently stable [23], [48]. Thus, $G(s)$ and $H(s)$ have no RHP poles, i.e., $N_{\mathrm{p,o}}=0$. On this premise, SC 3B can be derived as follows.

SC 3B: the closed-loop power system is stable when $N_{\mathrm{r}}=0$; otherwise, the system is unstable.

If $L(\mathrm{j}\omega)$ is an single-input single-output (SISO) function, SC 3A/3B can be adopted directly. If $L(\mathrm{j}\omega)$ is an MIMO function, a generalized Nyquist criterion can be employed [22], [23], [65], [66]. Specifically, the eigenvalues of the MIMO $L(\mathrm{j}\omega)$ can be calculated at each frequency point. Several SISO frequency characteristics of the eigenvalues can be derived. Then, SC 3A/3B can be adopted to the eigenvalue loci, thereby analyzing the small-signal stability of the MIMO closed-loop power system.

Based on Nyquist plots, potential OMs can be identified by OMIC 3.

OMIC 3 [22], [66]: the oscillation frequency is the frequency where the locus of $L(\mathrm{j}\omega)$ intersects the unit circle, i.e., $\omega/(2\pi)$ Hz that satisfies (14). The stability margin of an oscillation can be evaluated by the corresponding phase margin. For a stable oscillation, the larger the corresponding phase margin is, the more stable the oscillation is. The oscillation is critically stable when the phase margin is 0°.

$$\left|L(\mathrm{j}\omega)\right|=\left|G(\mathrm{j}\omega)H(\mathrm{j}\omega)\right|=1 \tag{14}$$

where $|\cdot|$ denotes the modulus.

As shown in Fig. 2(a), it should be pointed out that not all intersection points are valid for determining the oscillation frequencies. Only the intersection points close to $(-1,\mathrm{j}0)$ are meaningful, and the corresponding frequencies are close to the true oscillation frequencies [50]. Taking an SISO system as an example, the reasons are given as follows. Equation (15) can be satisfied only when s is a pole of the CLTF.

$$1+L(s)=0 \tag{15}$$

For a pole $s_1=\sigma_1\pm\mathrm{j}\beta_1$, $L(s_1)$ equals to $(-1,\mathrm{j}0)$. If σ_1 is small enough to make $\sigma_1\pm\mathrm{j}\beta_1\approx 0\pm\mathrm{j}\beta_1$, (16) can be achieved.

$$L(\mathrm{j}\beta_1)\approx L(\sigma_1\pm\mathrm{j}\beta_1)=(-1,\mathrm{j}0) \tag{16}$$

When (16) is satisfied for an OM, the corresponding intersection may be found nearby $(-1,\mathrm{j}0)$ in Nyquist plots. If $\sigma_1\pm\mathrm{j}\beta_1$ is not approximate to $0\pm\mathrm{j}\beta_1$, (16) may not be satisfied. Poles that do not satisfy the above condition cannot be

found in the Nyquist plot, resulting in the neglection of non-critical oscillations. Hence, only the frequencies of critically stable/unstable oscillations can be determined by OMIC 3 correctly. It is difficult to give a specific threshold that can determine whether an intersection point is close to $(-1, \mathrm{j}0)$ enough since the standard varies with OMs and operating conditions.

Nyquist plots are a kind of graphical method in frequency domain. The small-signal stability of a closed-loop PEDPS can be identified correctly on the premise that the number of the RHP poles of $G(s)H(s)$ is known. Moreover, the order of the PEDPS model is high due to the increasing number of power electronic devices. Hence, the Nyquist plots may become too complex to clearly check the encirclements in the PEDPS, which may limit the application of the Nyquist plots.

D. Bode Plot Based Methods

The Bode plots can be regarded as another form of Nyquist plots. A Bode plot consists of a magnitude-frequency plot and a phase-frequency plot. Based on the Bode plot of $L(\mathrm{j}\omega)$, the small-signal stability can be judged by SC 4 [23], [67], [68].

SC 4: the closed-loop power system is stable if the magnitude and phase of $L(\mathrm{j}\omega)$ satisfy (17).

$$\begin{cases} M\left(\left|L(\mathrm{j}\omega)\right|\right) < 0 \\ \angle L(\mathrm{j}\omega) = -180° \pm N_{\text{phase}} \cdot 360° \end{cases} \tag{17}$$

$$M(\cdot) = 20\lg(\cdot) \tag{18}$$

where N_{phase} is an integer; and $M\left(\left|L(\mathrm{j}\omega)\right|\right)$ and $\angle L(\mathrm{j}\omega)$ are the magnitude and phase of $L(\mathrm{j}\omega)$, respectively.

As Fig. 2(b) shows, the condition in (17) can also be rewritten as:

$$\begin{cases} M\left(\left|L(\mathrm{j}\omega)\right|\right) \geq 0 \\ \angle L(\mathrm{j}\omega) \neq -180° \pm N_{\text{phase}} \cdot 360° \end{cases} \tag{19}$$

In fact, SC 4 can be derived from SC 3B, which is regarded as a simplified Nyquist stability criterion. It should be noted that SC 4 is a sufficient and unnecessary condition for small-signal stability. This is because there may be a frequency, where $\angle L(\mathrm{j}\omega)$ satisfies (17) but $M\left(\left|L(\mathrm{j}\omega)\right|\right) > 0$ in a stable closed-loop power system. This case can be observed if $L(\mathrm{j}\omega)$ crosses the negative real axis to the left of -1 but does not encircle $(-1, \mathrm{j}0)$ in the corresponding Nyquist plot, as shown by the purple lines in Fig. 2 [23], [68]. Thus, SC 4 is conservative.

Similar to the Nyquist plot based methods, the potential OMs can be determined based on Bode plots as follows [67].

OMIC 4: the oscillation frequency is the frequency where the magnitude of $L(\mathrm{j}\omega)$ satisfies (20). For a stable oscillation, the larger the corresponding phase margin is, the more stable the oscillation is. The oscillation is critically stable when the phase margin is 0°.

$$M\left(\left|L(\mathrm{j}\omega)\right|\right) = 0 \tag{20}$$

The same as the analysis in Section III-C, OMIC 4 shares the same limitation in the PEDPS as OMIC 3. Different from the Nyquist plot based methods, SC 4 can only be employed on the premise that $G(s)H(s)$ have no RHP poles. Compared with the Nyquist plot based methods, the Bode plot based methods are more intuitive in a high-order PEDPS. In addition, the Bode plot based methods can be employed to analyze an MIMO PEDPS that is decoupled by the generalized Nyquist method [23].

E. Impedance-/Admittance-based Methods

For convenience, the impedance-/admittance-based methods are hereafter named impedance-based, as impedance and admittance can be easily converted to each other. The impedance-based methods gain interest from manufacturers and operators in a PEDPS since it is possible to model the power electronic devices without full information [7], [40], [48], [50], [67]. The impedance model of the PEDPS can be constructed in s domain or frequency domain. Moreover, the impedance model in frequency domain can be derived by frequency scanning, online measurement, etc., thereby reducing the difficulty in modeling [69], [70]. The core of impedance-based methods is to determine the transfer functions of a PEDPS based on impedance models. There are several forms to achieve it as follows.

A PEDPS can be divided into two subsystems at a point of common coupling (PCC). Especially, for a power system with converters, the converters at the same location and the rest of the power system can be regarded as two subsystems to analyze the oscillations between the converters and the rest of the power system [39].

A PEDPS described by a Thevenin equivalent circuit connected with a Norton equivalent circuit is taken as an example, as shown in Fig. 3(a).

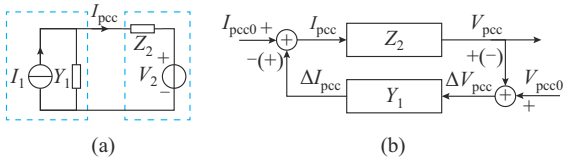

(a) (b)

Fig. 3. Different impedance-based small-signal stability analysis models. (a) Impedance model 1. (b) Impedance model 2.

In Fig. 3(a), the current between the two sub-circuits can be derived by [23], [48]:

$$I_{\text{pcc}}(s) = \left(1 + Y_1(s)Z_2(s)\right)^{-1}\left(I_1(s) - Y_1(s)V_2(s)\right) \tag{21}$$

where $I_{\text{pcc}}(s)$ is the current at PCC from the Norton equivalent circuit to the Thevenin equivalent circuit; $Y_1(s)$ and $I_1(s)$ are the equivalent admittance and current source in the Norton equivalent circuit, respectively; and $Z_2(s)$ and $V_2(s)$ are the equivalent impedance and voltage source in the Thevenin equivalent circuit, respectively.

If two assumptions are satisfied (i.e., $V_2(s)$ is stable, and the system is stable when $Z_2(s)$ is zero), the CLTF of the whole PEDPS can be expressed as [23]:

$$F_1(s) = \left(1 + Z_2(s)Y_1(s)\right)^{-1} \tag{22}$$

where the input is $I_1(s)-Y_1(s)V_2(s)$ and output is $I_{pcc}(s)$.

In addition, there is another form to get a CLTF based on the transfer functions of the two subsystems, as shown in Fig. 3(b) [15], [16], [39], [71]. The two subsystems can be described by two groups of state-space equations, like the forms in (6). By making voltage V_{pcc} (current I_{pcc}) as input $\boldsymbol{U}$ and making current I_{pcc} (voltage V_{pcc}) as output $\boldsymbol{W}$, the transfer functions of the two subsystems can be regarded as an admittance $Y_1(s)$ (impedance $Z_2(s)$) as:

$$Y_1(s) \text{ or } Z_2(s)=\boldsymbol{C}(s\boldsymbol{I}-\boldsymbol{A})^{-1}\boldsymbol{B}+\boldsymbol{D} \tag{23}$$

By setting V_{pcc0} and I_{pcc} (or I_{pcc0} and V_{pcc}) as the input and output of the CLTF, respectively, the CLTF can be expressed by (24) or (25) [16].

$$F_2(s)=\left(1+Y_1(s)Z_2(s)\right)^{-1}Y_1(s) \tag{24}$$

$$F_3(s)=\left(1+Z_2(s)Y_1(s)\right)^{-1}Z_2(s) \tag{25}$$

Although the CLTFs in (22), (24), and (25) seemingly have different forms, they share the same poles without considering ZPC. After deriving the impedance-based transfer functions of the PEDPS, various methods can be utilized to analyze the small-signal stability as follows.

1) Pole-based Analysis for Impedance Models

The poles of the impedance-based CLTF can be calculated. Then, SC 1 and OMIC 1 can be adopted to analyze the small-signal stability, as introduced in Section III-A.

2) Nyquist/Bode Plot Based Analysis for Impedance Models

According to the CLTFs in (22), (24), and (25), the OLTF in frequency domain can be derived as:

$$L(\mathrm{j}\omega)=Y_1(\mathrm{j}\omega)Z_2(\mathrm{j}\omega) \text{ or } L(\mathrm{j}\omega)=Z_2(\mathrm{j}\omega)Y_1(\mathrm{j}\omega) \tag{26}$$

Then, the generalized Nyquist plot and Bode plot of $L(\mathrm{j}\omega)$ can be drawn for further analysis by SC 3A/3B, SC 4, OMIC 3, and OMIC 4.

In addition, several derived sufficient and unnecessary criteria have been proposed, including Middlebrook criterion [72], gain and phase margin criterion [73], opposing argument criterion [74], and energy source analysis consortium (ESAC) criterion [74]. Different forbidden regions are introduced in these criteria. $L(\mathrm{j}\omega)$ is limited in the forbidden regions to guarantee the stability of a PEDPS. The comparison of different forbidden region boundaries is given in Fig. 4.

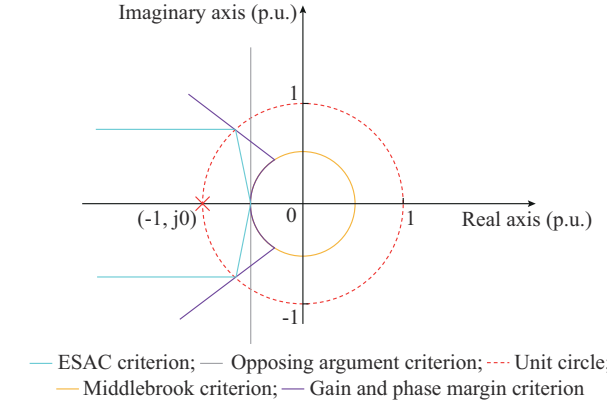

Fig. 4. Different forbidden region boundaries in s plane.

In Middlebrook criterion [72], $L(\mathrm{j}\omega)$ is required to satisfy:

$$\left|L(\mathrm{j}\omega)\right| \ll 1 \tag{27}$$

The gain and phase margin criterion defines a forbidden region by (28) [73]:

$$\begin{cases}\left|L(\mathrm{j}\omega)\right| > M_G^{-1} \\ -180°+M_P<\angle L(\mathrm{j}\omega)<180°-M_P\end{cases} \tag{28}$$

where M_G and M_P are the defined gain margin and phase margin, which are 2 and 60° in [73], respectively.

The opposing argument criterion proposes a forbidden region defined by [74]:

$$\mathrm{Re}\left(L(\mathrm{j}\omega)\right) \le -M_G^{-1} \tag{29}$$

where $\mathrm{Re}(\cdot)$ denotes the value of real part.

In ESAC criterion [75], the boundary of the forbidden region consists of two lines starting from negative infinity and paralleling the real axis. The two lines terminate at the unit circle and are connected by lines from the intersection points to $\left(-M_G^{-1}, \mathrm{j}0\right)$, as shown in Fig. 4.

These criteria can be regarded as simplified SC 3B rather than SC 3A since the stability is guaranteed by no encirclement of $(-1, \mathrm{j}0)$. They are design-oriented for easily guiding the design of the individual electronic component. Therefore, all these criteria are conservative.

3) Passivity-based Method

Taking the impedance model of a PEDPS shown in Fig. 3(a) as an example, the passivity of subsystem Y_1 (or Z_2) can be judged as follows [31]-[35]. The subsystem is passive if ① all poles of $Y_1(s)$ (or $Z_2(s)$) are in the left-half-plane; and ② $\mathrm{Re}\left(Y_1(\mathrm{j}\omega)\right)$ (or $\mathrm{Re}\left(Z_2(\mathrm{j}\omega)\right)$) is nonnegative for $\forall\omega$. Based on the concept of passivity, the small-signal stability of the whole power system can be identified as follows [31]-[35].

SC 5: the closed-loop power system is stable if all open-loop subsystems are passive.

The passivity of $Y_1(\mathrm{j}\omega)$ and $Z_2(\mathrm{j}\omega)$ indicates that $\angle L(\mathrm{j}\omega)$ is within $[-180°, 180°]$, thereby guaranteeing that the Nyquist plot does not encircle the point $(-1, \mathrm{j}0)$ [34], [35]. However, a stable system allows a case that the point $(-1, \mathrm{j}0)$ is not encircled, and meanwhile, $\angle L(\mathrm{j}\omega)$ is beyond $[-180°, 180°]$. Hence, SC 5 is a sufficient and unnecessary criterion for small-signal stability. The passivity-based method argues that the frequency ranges with negative $\mathrm{Re}\left(Y_1(\mathrm{j}\omega)\right)$ and $\mathrm{Re}\left(Z_2(\mathrm{j}\omega)\right)$ are related to potential resonance destabilization. Then, the stability of the whole power system can be improved by minimizing the negative-real-part ranges.

4) Positive-net-damping Method

The positive-net-damping method can be proven as a simplified representation of the Nyquist stability criterion [36]. Based on (26), if $Z_2(s)$ and $Y_1(s)$ have no RHP poles, the sufficient conditions for a stable PEDPS derived from SC 3B can be expressed as:

$$\begin{cases} \mathrm{Re}\left(Z_2(\mathrm{j}\omega)Y_1(\mathrm{j}\omega)\right) > -1 \\ \mathrm{Im}\left(Z_2(\mathrm{j}\omega)Y_1(\mathrm{j}\omega)\right) = 0 \end{cases} \tag{30}$$

where $\mathrm{Im}(\cdot)$ denotes the value of imaginary part; and $Y_1(\mathrm{j}\omega)$ and $Z_2(\mathrm{j}\omega)$ can be expressed by (31) and (32), respectively.

$$Y_1^{-1}(\mathrm{j}\omega) = Z_1(\mathrm{j}\omega) = R_1(\omega) + \mathrm{j}X_1(\omega) \tag{31}$$

$$Z_2(\mathrm{j}\omega) = R_2(\omega) + \mathrm{j}X_2(\omega) \tag{32}$$

where R_1, R_2 and X_1, X_2 are the resistances and reactances of subsystem 1 and subsystem 2, respectively.

By substituting (31) and (32) into (30), we can yield [36], [39]:

$$\begin{cases} R_1(\omega) + R_2(\omega) > 0 \\ \dfrac{X_2(\omega)}{X_1(\omega)} = \dfrac{R_2(\omega)}{R_1(\omega)} \end{cases} \tag{33}$$

Therefore, the positive-net-damping criterion can be expressed as follows [36], [39].

SC 6: the closed-loop power system is stable if (33) is satisfied.

The potential OMs can be identified as follows [37], [39].

OMIC 6: the oscillation frequency is the frequency where $\mathrm{Im}\left(Z_2(\mathrm{j}\omega)Y_1(\mathrm{j}\omega)\right)$ is 0. At the oscillation frequency, the oscillation is stable if $R_1(\omega) + R_2(\omega)$ is larger than 0.

SC 6 and OMIC 6 mean that the impedance model is passive around oscillation frequencies, thereby guaranteeing stability. Similar to SC 4, the positive-net-damping criterion is sufficient and unnecessary for small-signal stability. In addition, not all frequencies of potential OMs can be correctly determined by OMIC 6. The positive-net-damping criterion is easy to apply in practice since the physical meaning is clear, and the contribution of each subsystem for stability can be evaluated. For an MIMO power system, the MIMO impedance needs to be decoupled into SISO impedance, and then the passive-net-damping method can be employed [38], [39].

5) Lumped Impedance-based Method

In [40], a lumped impedance-based method is proposed to analyze the small-signal stability. The whole PEDPS can be represented by an impedance network model. Through circuit transformation, the impedance network model can be reduced into a lumped impedance Z_{LIM} or a lumped admittance Y_{LIM} in frequency domain. Taking Z_{LIM} as an example, a response current occurs by injecting a small voltage disturbance into the network, as shown in (34).

$$I_{\mathrm{out}}(\mathrm{j}\omega) = V_{\mathrm{in}}(\mathrm{j}\omega)Z_{\mathrm{LIM}}^{-1}(\mathrm{j}\omega) \tag{34}$$

where $Z_{\mathrm{LIM}}(\mathrm{j}\omega)$ is the frequency response of the CLTF for the power system.

Taking the impedance model shown in Fig. 3(a) as an example, Z_{LIM} can be derived by:

$$Z_{\mathrm{LIM}}(\mathrm{j}\omega) = Y_1^{-1}(\mathrm{j}\omega) + Z_2(\mathrm{j}\omega) = R_{\mathrm{LIM}}(\omega) + \mathrm{j}X_{\mathrm{LIM}}(\omega) \tag{35}$$

where $R_{\mathrm{LIM}}(\omega)$ and $X_{\mathrm{LIM}}(\omega)$ are the real part and imaginary part of $Z_{\mathrm{LIM}}(\mathrm{j}\omega)$, i. e., lumped resistance and lumped reactance, respectively.

It is assumed that oscillations with corresponding eigenvalues $\sigma \pm \mathrm{j}\beta$ can satisfy:

$$|\sigma| \ll |\beta| \tag{36}$$

It means that the oscillations are critically stable/unstable. In this case, the small-signal stability can be analyzed based on $R_{\mathrm{LIM}}(\omega)$ and $X_{\mathrm{LIM}}(\omega)$, as follows [40].

SC 7: the oscillation at a frequency ω is stable when (37) is satisfied; otherwise, the oscillation is unstable.

$$\begin{cases} R_{\mathrm{LIM}}(\omega)\dfrac{\mathrm{d}X_{\mathrm{LIM}}(\omega)}{\mathrm{d}\omega} > 0 \\ X_{\mathrm{LIM}}(\omega) = 0 \end{cases} \tag{37}$$

The potential OMs satisfying (36) can be identified as follows [41].

OMIC 7: the oscillation frequency is the frequency where $X_{\mathrm{LIM}}(\omega)$ is 0. The stability margin of the oscillation can be preliminarily assessed by $|R_{\mathrm{LIM}}(\omega)|$ at the oscillation frequency. The larger $|R_{\mathrm{LIM}}(\omega)|$ at the oscillation frequency is, the more stable (unstable) the corresponding oscillation is.

In (37), the zero-crossing points on $X_{\mathrm{LIM}}(\omega)$ can not only be caused around the frequencies of zeros but also the frequencies of poles. Oscillations are related to the zeros of $Z_{\mathrm{LIM}}(s)$ according to (34). Thus, only the zero-based zero-crossing points are valid for using SC 7 and OMIC 7. An experience-based judgment method is to observe the absolute value of the slope of $X_{\mathrm{LIM}}(\omega)$ at the zero-crossing point. If the value is relatively small, the zero-crossing point is caused by a zero [40].

In some special cases, the oscillation-related zero-crossing point can be caused on $R_{\mathrm{LIM}}(\omega)$. In this case, the oscillation is stable if (38) can be satisfied [40].

$$\begin{cases} X_{\mathrm{LIM}}(\omega)\dfrac{\mathrm{d}R_{\mathrm{LIM}}(\omega)}{\mathrm{d}\omega} < 0 \\ R_{\mathrm{LIM}}(\omega) = 0 \end{cases} \tag{38}$$

Similarly, only the zero-based zero-crossing points are valid. The details can be found in [40].

In practice, $Z_{\mathrm{LIM}}(\mathrm{j}\omega)$ is usually a 2×2 matrix in the *dq* frame. In this case, the form of (39) or (40) can be employed to analyze the small-signal stability [40], [42].

$$Z_{\mathrm{LIM,D}} = Z_{\mathrm{LIM},11}Z_{\mathrm{LIM},22} - Z_{\mathrm{LIM},21}Z_{\mathrm{LIM},12} \tag{39}$$

$$Z_{\mathrm{LIM,avg}} = \frac{1}{2}\left[\left(Z_{\mathrm{LIM},11} + Z_{\mathrm{LIM},22}\right) + \mathrm{j}\left(Z_{\mathrm{LIM},21} - Z_{\mathrm{LIM},12}\right)\right] \tag{40}$$

where $Z_{\mathrm{LIM},ik}$ is the element in the i^{th} row and the k^{th} column of $\boldsymbol{Z}_{\mathrm{LIM}}$. Equation (40) is only available for the symmetrical or slightly asymmetrical impedance [42].

Through the lumped impedance-based method, the potential OMs can be identified without computing zeros or poles. Therefore, the method is easy to apply in practice. However, the preconditions of this method limit the analysis of non-critically stable/unstable oscillations.

F. Bifurcation-based Method

In theory, bifurcation is the appearance of a new pattern, e.g., instability, caused by the continuous changes of parameters in a PEDPS [46], [76]. Thus, the structural stability can

be analyzed by the bifurcation-based method. Specifically, the dynamics of a PEDPS can be described by DAEs like (1) with parameters $\boldsymbol{p}_s$ [46]. After linearizing DAEs, the state matrix $\boldsymbol{A}_s$ can be derived as (4). The small-signal stability can be judged by the eigenvalues of $\boldsymbol{A}_s$, which depends on $\boldsymbol{p}_s$. Therefore, a bifurcation can be regarded as a specific set of $\boldsymbol{p}_s$ that can make the PEDPS marginally stable/unstable.

In the small-signal stability analysis, there are mainly Hopf bifurcation, saddle-node bifurcation, singularity-induced bifurcation, and limit-induced bifurcation [43], [44]. Among them, the Hopf bifurcation is related to the oscillatory stability since it is caused by the move of a pair of complex conjugate eigenvalues [45]. A Hopf bifurcation can be identified by checking the requirements as [46]:

$$\begin{cases} \boldsymbol{f}\left(\boldsymbol{x}_c, \boldsymbol{y}_c, \boldsymbol{p}_{HB}\right) = \boldsymbol{0} \\ \boldsymbol{g}\left(\boldsymbol{x}_c, \boldsymbol{y}_c, \boldsymbol{p}_{HB}\right) = \boldsymbol{0} \end{cases} \tag{41}$$

$$\lambda_{HB} = \pm \mathrm{j}\beta \tag{42}$$

$$\frac{\mathrm{d}}{\mathrm{d}\boldsymbol{p}} \mathrm{Re}\left(\lambda\left(\boldsymbol{p}_{HB}\right)\right) \neq 0 \tag{43}$$

where $\boldsymbol{x}_c \in \mathbb{R}^n$ and $\boldsymbol{y}_c \in \mathbb{R}^m$ are the vectors of the dynamic variables and algebraic variables at the current equilibrium point, respectively; $\boldsymbol{p}_{HB} \in \mathbb{R}^v$ is the value of $\boldsymbol{p}_s$ under the bifurcation condition, i.e., Hopf bifurcation value; and only a pair of conjugate eigenvalues λ_{HB} can satisfy (42).

The requirements above describe the crossing of a complex conjugate pair of eigenvalues on the imaginary axis. By identifying or predicting the bifurcations, the parameter space can be divided into a stable region and an unstable region, thereby providing guidance on evaluating and improving the small-signal stability. The bifurcation-based method still relies on other analysis methods, e.g., the eigenvalue/pole based methods, to evaluate the stability at specific system parameters.

IV. Discussions on Different Small-signal SC

A. Connection and Discrepancy Between Multiple Criteria

The above methods can be divided into time-domain-based methods, *s*-domain-based methods, and frequency-domain-based methods according to employed models. The connections between these criteria are demonstrated in Fig. 5.

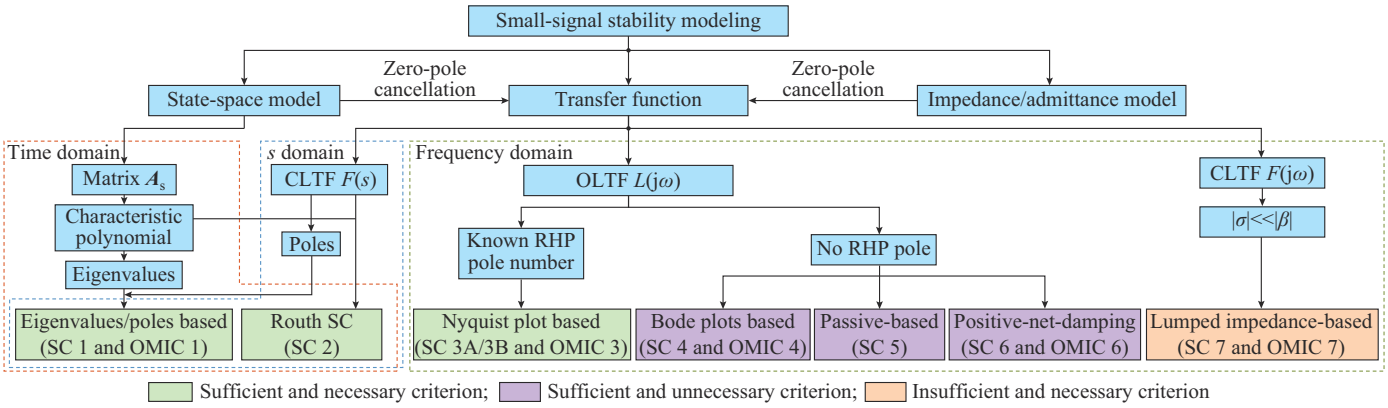

Fig. 5. Connections among different small-signal SCs.

Emerging issues have been induced in the PEDPS, including aspects from black-box modeling, high model dimension, wideband frequency characteristics, and new oscillation mechanisms, for the covered methods. These issues seriously affect the effective application of the above methods, which are analyzed in detail as follows.

The time-domain-based methods analyze the small-signal stability by computing eigenvalues via state-space models, requiring a thorough knowledge of the structure and parameters of the system.

A main challenge induced by the converters is how to obtain an accurate state-space model and solve effective eigenvalues [49], [53], [77]. Different from conventional components (e.g., SGs and transformers) that have matured and standard analytical models, the converters lack standard models since the characteristics are mainly determined by their control structures and algorithms. The detailed structure and algorithm of a converter are usually kept confidential by the manufacturer to protect intellectual property, thereby further hindering the accurate state-space model of the converter. In this case, [78] provides an optional solution to estimate the state-space representation for the converter. An estimated transfer function in *s* domain is regarded as an approximation of the state-space model. By modeling the black-box converter as RLC branches, the parameters of the RLC branches can be computed from the pole/residue values of the estimated transfer function in *s* domain. Then, the converter is represented by a state-space model of the RLC branches. It should be noted that the relationships between the parameters in the RLC branches and real control parameters may not be clearly observed, resulting in difficulty in stability optimization. Hence, the state-space modeling for the black-box converters still needs further research and breakthroughs.

In addition, the order of the state transform matrix may be extremely high. The dynamics of a converter in electromagnetic time-scale should be considered in the state-space model, resulting in a high order for the device model. Meanwhile, there are far more converters than SGs in the PEDPS. Hence, the detailed state-space model for a large-scale multi-

machine power system with converters is super high order, resulting in the difficulty in effectively solving eigenvalues and explaining the model intuitively in terms of physical meaning [49]. The formation of the state-space model of the whole power system with massive converters can be simplified by a component connection method (CCM), but the model order is still high [79]. The model order reduction is a solution that is worth further studying for improving the solvability of eigenvalues [80].

When the system is unbalanced or harmonic interaction of converters is considered [49], [53], the linearized model can be time-periodic and cannot be employed for eigenvalue analysis directly. Some emerging methods including DP [55], [56] and HSS [49], [57] may provide potential solutions in this case.

The *s*-domain-based methods analyze the small-signal stability by computing poles via a CLTF with respect to a complex argument *s*. Mathematically, a unique transfer function can be derived from a state-space model. SC 1, OMIC 1, and SC 2 are valid for both the time-domain-based methods and the *s*-domain-based methods.

The *s*-domain-based methods are one of the most popular methods for small-signal stability analysis in the PEDPS. The *s*-domain model of a black-box converter can be regarded as an impedance without knowing the inner details. A solution to model the black-box converter is to estimate the *s*-domain model from measurement data or simulation by estimating techniques, e.g., vector fitting [58], [59]. The linearized time-periodic characteristics can be modeled by harmonic linearization [53], [54] and harmonic transfer function [49], [57] techniques. It should be pointed out that the order of the estimated *s*-domain model is usually determined manually, thereby resulting in estimation errors and spurious poles [81], [82]. The fitting errors of different devices may be further cumulated into the system model. Hence, the large-scale use of estimated *s*-domain models should be done with caution. The Routh stability criterion only gives the number of poles with non-negative real parts, and thus the effects of the estimated errors and spurious poles can hardly be noticed and mitigated.

Noticeably, ZPC may be caused when forming a transfer function, affecting the analysis results. The impedance-based transfer functions are widely employed in small-signal stability analysis of the PEDPS, which suffer from the ZPC issue. Different forms of CLTFs consisting of $Y_1(s)$ and $Z_2(s)$ can be expressed by (22), (24), (25), and the inversion of (35). $Y_1(s)$ and $Z_2(s)$ can be expressed by corresponding pole polynomials (P_{p1} and P_{p2}) and zero polynomials (P_{z1} and P_{z2}) as:

$$Y_1(s) = \frac{P_{z1}(s)}{P_{p1}(s)} \tag{44}$$

$$Z_2(s) = \frac{P_{z2}(s)}{P_{p2}(s)} \tag{45}$$

By substituting (44) and (45) into (22), (24), (25), and the inversed (35), we can yield:

$$F_1(s) = \frac{P_{p2}(s)P_{p1}(s)}{P_{z2}(s)P_{z1}(s)+P_{p2}(s)P_{p1}(s)} \tag{46}$$

$$F_2(s) = \frac{P_{z1}(s)P_{p2}(s)}{P_{z2}(s)P_{z1}(s)+P_{p2}(s)P_{p1}(s)} \tag{47}$$

$$F_3(s) = \frac{P_{z2}(s)P_{p1}(s)}{P_{z2}(s)P_{z1}(s)+P_{p2}(s)P_{p1}(s)} \tag{48}$$

$$\frac{1}{Z_{LIM}(s)} = \frac{P_{z1}(s)P_{p2}(s)}{P_{z1}(s)P_{z2}(s)+P_{p1}(s)P_{p2}(s)} \tag{49}$$

Obviously, the four different forms of CLTFs have the same poles without considering the ZPC issue. Essentially, different approaches for forming CLTFs generate different closed-loop zeros. The closed-loop zeros consist of open-loop zeros and/or poles. It can be inferred that once an OM in a subsystem is not affected by the forming of the closed loop, the corresponding open-loop poles and closed-loop poles are the same. In this case, if the open-loop poles belong to the pole polynomials existing in the numerator part of a CLTF, the corresponding closed-loop poles can be cancelled. A recommended approach to solve the issue is to form the CLTF by dividing the whole PEDPS at different PCCs [63]. Then, the analysis results of different CLTFs can be comprehensively considered.

Although eigenvalues and poles can provide detailed and accurate analysis results for oscillations, detailed state-space models or *s*-domain transfer functions of the PEDPS are required. Similar to the *s*-domain model, the frequency-domain model of a black-box converter can also be derived from measurement data or simulation data [40], [48]. However, the additional step of estimating techniques, e.g., vector fitting [58], [59], is not necessary, and thus the frequency-domain modeling is easier to realize compared with the *s*-domain modeling.

The small-signal stability of the whole PEDPS can be determined correctly based on Nyquist plots if the number of the open-loop RHP poles is known. Moreover, if the open-loop subsystems are stable, Bode plots and the positive-net-damping method can also be employed, which are conservative. Guaranteeing the requirements of RHP pole number is challenging in the PEDPS, since the control parameters of a converter may change with operating points and interactions within the subsystem may cause instability [83], [84]. By contrast, the knowledge about the number of open-loop RHP poles is not required by the lumped impedance-based method since it is based on the CLTF essentially. However, the non-critically stable/unstable oscillations may not be identified by the lumped impedance-based method. Although the non-critically stable/unstable oscillations also may not be identified by the Nyquist/Bode plot based and positive-net-damping methods, the impacts of these non-critical oscillations can still be considered when judging the stability of the whole power system.

B. Sufficiency and Necessity of Multiple Criteria on Stable Region

According to the above analysis, the stable regions given by different criteria are compared in Fig. 6, which aims to demonstrate the containment relationship of the stable/unstable regions defined by different criteria.

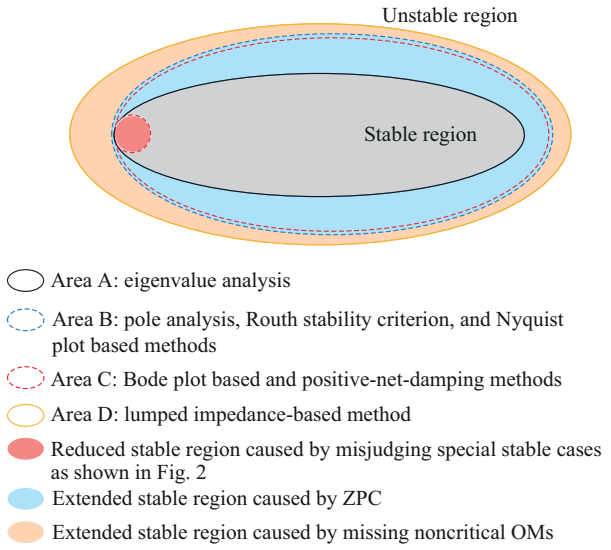

Fig. 6. Comparison of stable regions of different small-signal SC.

The grey area (Area A) presents the stable region determined by eigenvalue analysis. Area A is regarded as the actual stable region as SC 1 based on eigenvalues is the sufficient and necessary condition for stability.

Compared with the actual region, the stable region (Area B) determined by the pole analysis, Routh stability criterion, and Nyquist plot based methods is larger. The extended area is caused by the ZPC issue when deriving transfer functions. Without considering the ZPC issue, the corresponding criteria are sufficient and necessary for stability.

Compared with Area B, the stable region determined by the Bode plot methods and positive-net-damping methods (Area C) is reduced. The reason is that the special stable cases that $L(\mathrm{j}\omega)$ crosses the negative real axis to the left of -1 but does not encircle $(-1, \mathrm{j}0)$ in the complex plane can be misjudged as unstable cases by the methods of Area C but can still be accurately judged by the methods of Area B. Hence, a reduction of the stable region in Area C occurs due to the misjudgment of the special stable cases. The methods of Area C are sufficient but unnecessary without consideration of the ZPC issue. Compared with Area A, the extended stable region of Area C is caused by the ZPC issue.

Comparing the stable region (Area D) determined by the lumped impedance-based method with Area B, the extended stable region is caused by the assumption of (36). Non-critical OMs may not be identified, and thereby, more unstable cases may be misjudged. Compared with Area C, the actual stable region in Area D is extended because the special stable cases may be ignored but would not be misjudged by the lumped impedance-based method. Thus, it is necessary but insufficient for stability.

Generally, the accurate stable region can be provided by the eigenvalue analysis. If no unstable OMs are ignored by the ZPC, the accurate stable region can be provided by the pole analysis, Routh stability criterion, and Nyquist plot based methods. The Bode plot based methods, positive-net-damping method, and lumped impedance-based method can hardly provide an accurate stable region even if the impact of the ZPC is ignored.

According to the above discussions, the eigenvalue analysis and pole analysis are preferred if the required accurate state-space models or *s*-domain transfer functions can be derived easily. Otherwise, the frequency-domain-based methods are more applicable. Combining two or more frequency-domain-based methods is recommended to analyze wideband oscillations in the PEDPS due to their different limitations in stability judgment and OM identification. For example, after obtaining the impedance models in frequency domain, Nyquist/Bode plots based method and positive-net-damping method can be employed to guarantee the small-signal stability of the whole PEDPS. Meanwhile, the lumped impedance-based method can be adopted to identify potential critical wideband oscillations.

V. Case Study

To demonstrate and compare the performance of different small-signal stability analysis methods in PEDPSs, including eigenvalue/pole based methods, Nyquist/Bode plot based methods, and emerging impedance-based methods, two test power systems with different scales (modified 4-machine 2-area (4M2A) power system and modified IEEE 39-bus power system) are employed in this section.

A. Modified 4M2A Power System

The modified 4M2A power system with a permanent magnet synchronous generator (PMSG) based wind farm is employed as the test system. The single-line diagram of this test system is shown in Fig. 7.

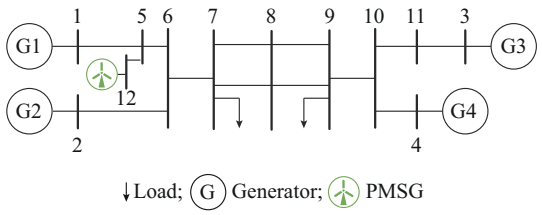

Fig. 7. Single-line diagram of modified 4M2A power system.

1) Eigenvalue-based Analysis in Modified 4M2A Power System

The system is modeled under the *dq*-frame. By dividing the whole power system into two subsystems at bus 12, the admittance of the PMSG-based subsystem $\boldsymbol{Y}_{\mathrm{PMSG1}}$ and the impedance of the rest of the power system $\boldsymbol{Z}_{\mathrm{ROPS1}}$ can be regarded as the corresponding transfer functions, respectively. Then, the CLTF can be derived according to (25), and the poles of the CLTF can be calculated. The obtained conjugate eigenvalues and poles are compared in Table I.

In addition to the conjugate eigenvalues/poles in Table I, all real eigenvalues/poles are negative. Hence, according to SC 1, the power system is stable because all the real parts of eigenvalues/poles are negative. However, compared with the eigenvalues, three pairs of poles can hardly be found since they are cancelled by zeros.

TABLE I
CONJUGATE EIGENVALUES AND POLES IN MODIFIED 4M2A POWER SYSTEM

Eigenvalue	Pole	Frequency (Hz)	Damping ratio (%)
−22.680±j97.89	−22.680±j97.89	15.58	22.57
−12.490±j69.68	−12.490±j69.68	11.09	17.64
−0.091±j9.87	−0.091±j9.87	1.57	0.92
−0.670±j5.80	−0.670±j5.80	0.92	11.48
−0.610±j5.78	−0.610±j5.78	0.92	10.50
−0.330±j3.09	−0.330±j3.09	0.49	10.62
−0.037±j0.82	−0.037±j0.82	0.13	4.51
−2.500±j22.22	None	3.54	11.18
−2.180±j22.21	None	3.53	9.77
−0.320±j1.55	None	0.25	20.22

2) Nyquist/Bode Plot Based Analysis in Modified 4M2A Power System

According to (26), the OLTF is $\boldsymbol{Y}_{\mathrm{PMSG1}}\boldsymbol{Z}_{\mathrm{ROPS1}}$. Two decoupled eigenvalue loci, i. e., $\lambda_{\mathrm{GNC},1}$ and $\lambda_{\mathrm{GNC},2}$, are derived by generalized Nyquist plot based method. Correspondingly, the generalized Nyquist plot and corresponding Bode plot are drawn in Fig. 8 and Fig. 9, respectively.

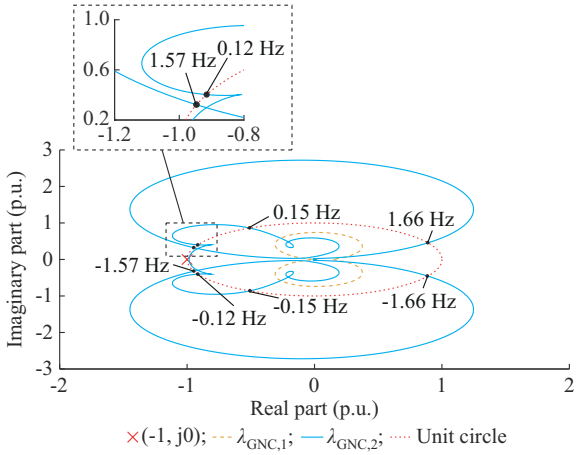

Fig. 8. Results of generalized Nyquist plot in modified 4M2A power system.

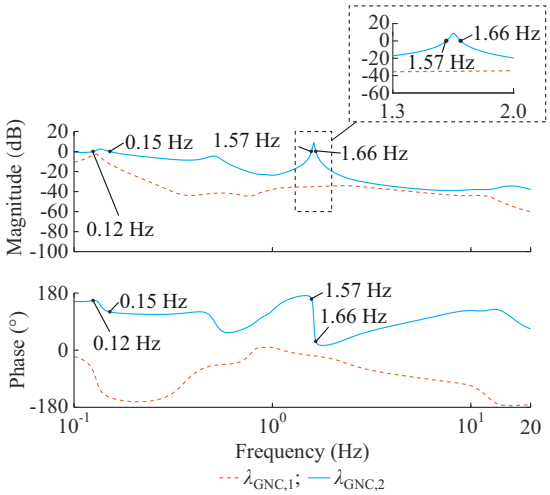

Fig. 9. Results of Bode plot in modified 4M2A power system.

$\boldsymbol{Z}_{\mathrm{ROPS1}}$ and $\boldsymbol{Y}_{\mathrm{PMSG1}}$ are designed to be stable. Thus, the power system is stable according to SC 3B and SC 4.

According to OMIC 3, eight intersections of the generalized Nyquist plot and the unit circle can be found. However, only the intersections close to (−1, j0) are available for identifying potential OMs. Hence, two OMs at 0.12 Hz and 1.57 Hz can be identified, corresponding to the eigenvalues with the smallest two stability margins, i. e., −0.037±j0.82 and −0.091±j9.87. According to OMIC 4, these two OMs can be identified in the Bode plot. The other OMs with higher stability margins cannot be identified through OMIC 3 and OMIC 4.

3) Emerging Impedance-based Analysis in Modified 4M2A Power System

In this part, the lumped impedance-based method is adopted. According to (35), the lumped impedance $\boldsymbol{Z}_{\mathrm{4M2A}}$ can be derived by $\boldsymbol{Z}_{\mathrm{ROPS1}}+\boldsymbol{Y}_{\mathrm{PMSG1}}^{-1}$. Then, based on (40), the 2×2 lumped impedance is approximately represented by a 1×1 impedance, as shown in Fig. 10.

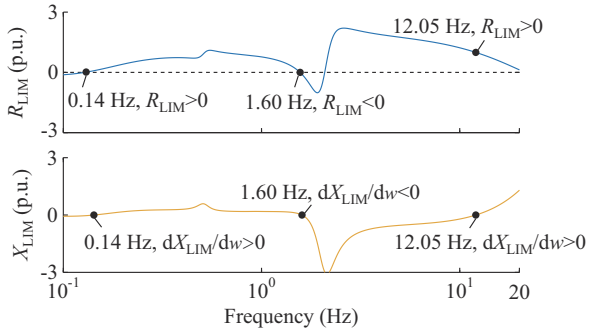

Fig. 10. Results of lumped impedance-based method in modified 4M2A power system.

There are three zero-based zero-crossing points on the X_{LIM} curve. According to OMIC 7, the identified oscillation frequencies are 0.14, 1.60, and 12.05 Hz, respectively. According to SC 7, the three oscillations are stable. The three OMs correspond to the eigenvalues −0.037±j0.82, −0.091± j9.87, and −12.490±j69.68, respectively. The frequencies of the first and second oscillations with small stability margins are almost the same as the actual frequencies derived from eigenvalues. Compared with the Nyquist/Bode plot based method, one more OM at around 11.09 Hz can be identified. However, the identified frequency is not very close to the actual frequency (12.05 Hz v.s. 11.09 Hz) since (36) can hardly be satisfied well.

The positive-net-damping method is applicable to an SISO system. There is no evidence supporting that the positive-net-damping method is available based on the approximate SISO impedance models like the lumped impedance-based method. However, the effectiveness of the positive-net-damping method can be inferred from the results of the Nyquist/Bode plots in Fig. 9 according to their interlinks revealed in the 4th part in Section III-E.

The lumped impedance-based method and the positive-net-damping method can share the same lumped resistance curve. For a stable oscillation, the lumped resistance is allowed to be positive or negative by the lumped impedance-

based method, but only allowed to be positive by the positive-net-damping method. This is because the oscillation frequencies identified by these two methods are different. The oscillation frequencies are identified through the zero-crossing points of the imaginary part of $\boldsymbol{Z}_{\mathrm{ROPS1}}+\boldsymbol{Y}_{\mathrm{PMSG1}}^{-1}$ in the lumped impedance-based method, while through the zero-crossing points of the imaginary part of $\boldsymbol{Z}_{\mathrm{ROPS1}}\boldsymbol{Y}_{\mathrm{PMSG1}}$ in the positive-net-damping method.

B. Modified IEEE 39-bus Power System

The modified IEEE 39-bus power system with 3 PMSG-based wind farms at buses 40, 41, and 42 is employed as the test system, as shown in Fig. 11.

1) Eigenvalue-based Analysis in Modified IEEE 39-bus Power System

By dividing the whole power system into two subsystems at bus 40, the admittance of the PMSG-based subsystem $\boldsymbol{Y}_{\mathrm{PMSG2}}$ and the impedance of the rest of the power system $\boldsymbol{Z}_{\mathrm{ROPS2}}$ can be regarded as the corresponding transfer functions, respectively. Then, the CLTF can be derived according to (25), and the poles of the CLTF can be calculated. The obtained conjugate eigenvalues and poles are compared in Table II.

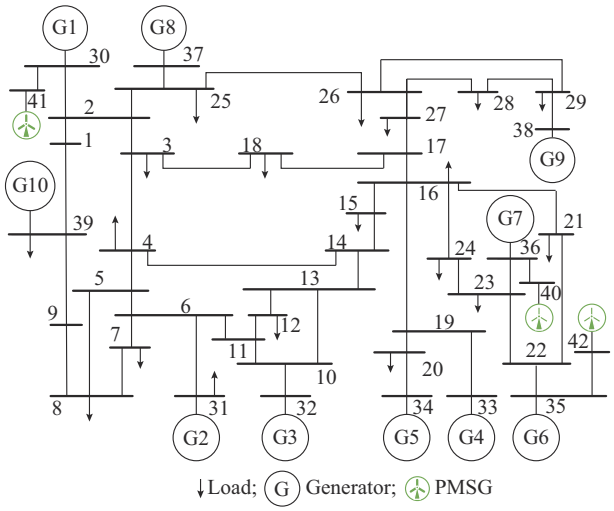

Fig. 11. Single-line diagram of modified IEEE 39-bus power system.

TABLE II
CONJUGATE EIGENVALUES AND POLES IN MODIFIED IEEE 39-BUS POWER SYSTEM

Eigenvalue	Pole	Frequency (Hz)	Damping ratio (%)	Eigenvalue	Pole	Frequency (Hz)	Damping ratio (%)
–22.070±j96.66	–22.070±j96.66	15.38	22.26	–0.071±j3.16	–0.071±j3.16	0.50	2.26
–20.640±j93.56	–20.640±j93.56	14.89	21.55	–0.091±j0.83	–0.091±j0.83	0.13	11.01
–12.420±j69.70	–12.420±j69.70	11.09	17.55	–0.088±j0.82	–0.088±j0.82	0.13	10.69
–12.430±j69.67	–12.430±j69.67	11.09	17.56	–0.088±j0.82	–0.088±j0.82	0.13	10.71
–12.430±j69.67	–12.430±j69.67	11.09	17.56	–3.790±j0.79	–3.790±j0.79	0.13	97.91
–0.106±j10.62	–0.106±j10.62	1.69	1.00	–2.500±j22.22	None	3.54	11.18
–0.110±j10.43	–0.110±j10.43	1.66	1.04	–2.500±j22.22	None	3.54	11.18
–0.190±j7.84	–0.190±j7.84	1.25	2.42	–2.500±j22.22	None	3.54	11.18
–0.160±j7.74	–0.160±j7.74	1.23	2.05	–2.440±j22.20	None	3.53	10.91
–0.350±j7.59	–0.350±j7.59	1.21	4.64	–2.440±j22.20	None	3.53	10.91
–0.028±j6.49	–0.028±j6.49	1.03	0.43	–2.440±j22.20	None	3.53	10.91
–0.099±j6.45	–0.099±j6.45	1.03	1.54	–0.063±j1.12	None	0.18	5.61
–0.160±j5.97	–0.160±j5.97	0.95	2.72	–0.063±j1.12	None	0.18	5.61
–0.040±j5.31	–0.040±j5.31	0.85	0.75	–0.063±j1.12	None	0.18	5.61
–1.440±j4.85	–1.440±j4.85	0.77	28.43				

In addition to the conjugate eigenvalues/poles in Table II, all real eigenvalues/poles are negative. Hence, according to SC 1, the power system is stable because all the real parts of eigenvalues/poles are negative. However, compared with the eigenvalues, nine pairs of poles can hardly be found since they are cancelled by zeros.

2) Nyquist/Bode Plot Based Analysis in Modified IEEE 39-bus System

According to (26), the OLTF is $\boldsymbol{Y}_{\mathrm{PMSG2}}\boldsymbol{Z}_{\mathrm{ROPS2}}$. The generalized Nyquist plot and corresponding Bode plot are drawn in Figs. 12 and 13, respectively.

$\boldsymbol{Z}_{\mathrm{ROPS2}}$ and $\boldsymbol{Y}_{\mathrm{PMSG2}}$ are designed to be stable. Thus, the power system is stable according to SC 3B and SC 4.

According to OMIC 3, 12 intersections of the generalized Nyquist plot and the unit circle can be found. However, only the intersections close to (–1, j0) are available for identifying potential OMs. Therefore, 3 OMs at 0.50, 0.85, and 1.66 Hz can be identified, corresponding to the conjugate eigenvalues –0.071±j3.16, –0.040±j5.31, and –0.110±j10.43, respectively. According to OMIC 4, these 3 OMs can be identified in the Bode plot. Other OMs cannot be identified through OMIC 3 and OMIC 4.

3) Emerging Impedance-based Analysis in Modified IEEE 39-bus Power System

In this part, the lumped impedance-based method is adopted. According to (35), the lumped impedance $\boldsymbol{Z}_{\mathrm{IEEE39}}$ can be derived by $\boldsymbol{Z}_{\mathrm{ROPS2}}+\boldsymbol{Y}_{\mathrm{PMSG2}}^{-1}$. Then, based on (40), the 2×2 lumped impedance is approximately represented by a 1×1 impedance, as shown in Fig. 14.

There are four zero-based zero-crossing points on the curve of X_{LIM}. According to OMIC 7, the identified oscillation frequencies are 0.51, 0.85, 1.66, and 18.74 Hz. The frequencies of the first 3 OMs (i.e., 0.51, 0.85, and 1.66 Hz) are quite close to the results of the Nyquist plot and Bode plot.

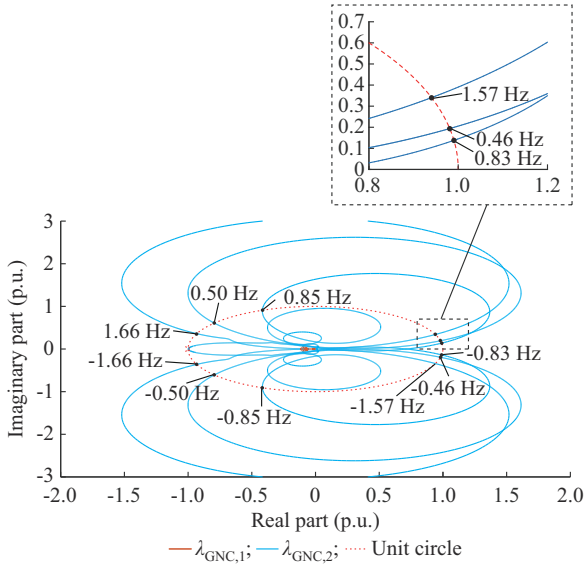

Fig. 12. Results of generalized Nyquist plot in modified IEEE 39-bus power system.

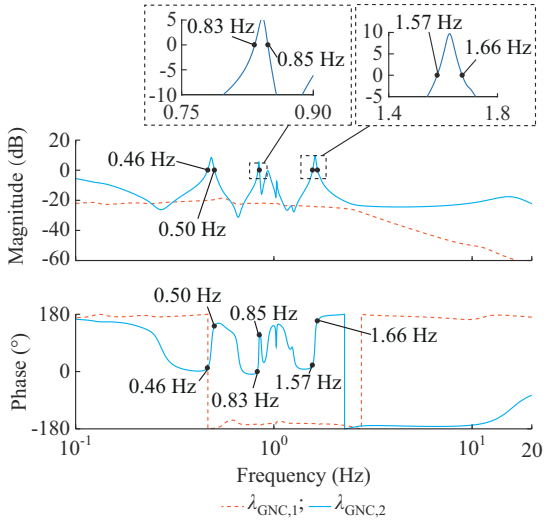

Fig. 13. Results of Bode plot in modified IEEE 39-bus power system.

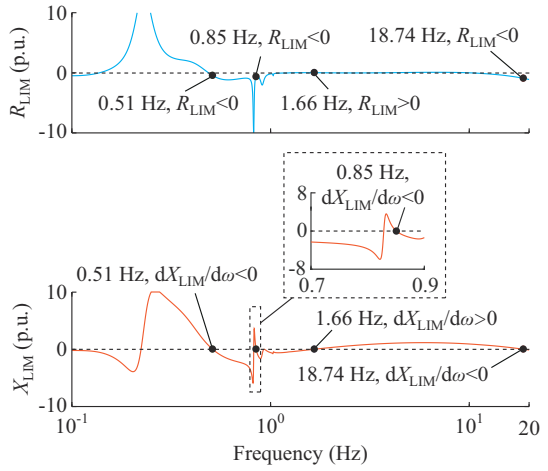

Fig. 14. Results of lumped impedance-based method in modified IEEE 39-bus power system.

However, the identified frequency of the last OM is not very close to the actual frequency (18.74 Hz v.s. 15.38 Hz) since (36) can hardly be satisfied. According to SC 7, the four identified oscillations are all stable.

The effects of the increasing scale of a PEDPS on results of different criteria can be analyzed by comparing the results in the two PEDPSs with different scales, as follows. By comparing the generalized Nyquist plots in the modified IEEE 39-bus power system and the modified 4M2A power system, the encirclements become growingly complex and difficult to count clearly due to the increasing order of the power system model. According to the OM identification results of different criteria in the two power systems with different scales, the number of OMs that can be successfully identified by existing criteria does not increase significantly as the number of actual potential OMs increases. It is indicated that the ability of existing criteria to identify potential OMs in a large-scale PEDPS still needs to be improved further, and otherwise, massive OMs may be ignored in the large-scale PEDPS.

VI. Challenges for Small-signal SC in PEDPSs

With the wide deployment of power electronics and renewable energy sources, the small-signal stability problems are not only limited to conventional LFOs but also involve wideband oscillations. In a future large-scale high-order PEDPS, thousands of OMs in a wide frequency range may be found. It is very challenging to analyze the small-signal stability and identify key OMs in such a power system. The increasing difficulty in small-signal modeling hinders the analysis based on state-space models and *s*-domain transfer functions. By contrast, the frequency-domain-based methods have great application potential for future PEDPS, while there are still many challenges to these methods.

The reviewed sufficient criteria in frequency domain rely on the knowledge of the number of open-loop RHP poles. In a PEDPS with thousands of OMs, it is challenging to analyze the small-signal stability when the number of open-loop RHP poles is unknown. Using an impedance-based CLTF is an effective and promising approach to solve the limitation of the strict assumption of no RHP poles compared with using an impedance-based OLTF.

All impedance-based methods suffer from the ZPC issue. Especially, different frequency responses can be generated by CLTFs with different forms even using the same impedance models of subsystems, which may result in neglecting some important OMs. Thus, there is a need to understand whether the frequency response associated with an oscillation is cancelled or weakened to avoid incorrect or incomplete results.

Nyquist stability criterion and its derivatives provide effective tools to analyze the stability of the whole PEDPS. However, the frequencies and stability margin of most potential oscillations can hardly be obtained by existing frequency-domain-based methods. Only some critically stable/unstable oscillations can be effectively found due to various strict assumptions. However, the structures and parameters of converters may change with operating points, thereby affecting

the induced oscillation. In this case, a non-critical converter-induced oscillation may have a large unstable risk and not be identified timely. Thus, using the frequency response to identify more oscillations deserves more effort.

Benefiting from the ability to use black-box converter models, the frequency-domain-based methods are widely employed in the PEDPS. The existing frequency-domain-based methods mainly provide the numerical results of stability, oscillation frequency, and margin, but may hardly give an insight into the mechanism of oscillations and formulate stability control strategies accordingly.

The frequency-domain modeling for a PEDPS usually relies on measurement technologies. The results of these criteria may be affected by measurement errors. Analyzing and mitigating the impacts of the errors is crucial for the large-scale application of frequency-domain-based small-signal stability analysis.

In general, more research efforts are expected to address the above emerging challenges in the future PEPDS.

VII. Conclusion

In this paper, the applicability of the eight types of small-signal stability analysis methods for PEDPSs is reviewed and compared. Regarding the accuracy of stability judgement and oscillation mode identification, the eigenvalues methods can provide the most accurate results. In *s* domain, the stability of a power system and potential OMs may not be fully identified correctly since the pole-based analysis can be affected by the ZPC issue. The Routh stability criterion can evaluate the stability but cannot provide the information of OMs. In frequency domain, the stability can be identified by the Nyquist stability criterion correctly if the number of RHP poles in open-loop systems is known. Based on the Nyquist stability criterion, the Bode plot based method and other design-oriented methods can be employed to analyze the stability conservatively. In the Nyquist/Bode plot, critical OMs can be identified through the intersections of the frequency response and unit circle/0 dB. Only the intersections close to point $(-1, j0)/-180°$ in the Nyquist/Bode plot are valid to identify potential OMs. These limitations are also valid for the positive-net-damping criterion. More critical OMs may be identified by the lumped impedance-based method, but the stability of the whole power system cannot be evaluated well. Nyquist plot based criterion (SC 3A/3B) is the only sufficient and necessary criterion among the introduced frequency-domain-based methods. The sufficiency and necessity of Bode plot based method, passivity-based method, and positive-net-damping method can be explained by the Nyquist plot based criterion.

Regarding modeling difficulty in the PEDPS, their ranking is inversed. The white-box state-space modeling in time domain is challenging in the PEDPS, while the *s*-domain modeling and frequency-domain modeling can be realized by impedance measurement techniques. Fitting errors and spurious poles may be generated when estimating *s*-domain models. Hence, the frequency-domain-based methods have the lowest implementation difficulty.

References

[1] Y. Cheng, L. Fan, J. Rose *et al*., "Real-world subsynchronous oscillation events in power grids with high penetrations of inverter-based resources," *IEEE Transactions on Power Systems*, vol. 38, no. 1, pp. 316-330, Jan. 2023.

[2] S. Bu, L. G. Meegahapola, D. P. Wadduwage *et al*., "Stability and dynamics of active distribution networks (ADNs) with D-PMU technology: a review," *IEEE Transactions on Power Systems*, vol. 38, no. 3, pp. 2791-2804, May 2023.

[3] H. Zhang, W. Xiang, W. Lin *et al*., "Grid forming converters in renewable energy sources dominated power grid: control strategy, stability, application, and challenges," *Journal of Modern Power Systems and Clean Energy*, vol. 9, no. 6, pp. 1239-1256, Nov. 2021.

[4] L. G. Meegahapola, S. Bu, D. P. Wadduwage *et al*., "Review on oscillatory stability in power grids with renewable energy sources: monitoring, analysis, and control using synchrophasor technology," *IEEE Transactions on Industrial Electronics*, vol. 68, no. 1, pp. 519-531, Jan. 2021.

[5] H. Liu, D. Sun, P. Song *et al*., "Influence of virtual synchronous generators on low frequency oscillations," *CSEE Journal of Power and Energy Systems*, vol. 8, no. 4, pp. 1029-1038, Jul. 2020.

[6] P. Kundur, *Power System Stability and Control*. New York: McGraw-Hill, 1994.

[7] M. Amin and M. Molinas, "Small-signal stability assessment of power electronics based power systems: a discussion of impedance- and eigenvalue-based methods," *IEEE Transactions on Industry Applications*, vol. 53, no. 5, pp. 5014-5030, Sept.-Oct. 2017.

[8] L. Fan, "Modeling type-4 wind in weak grids," *IEEE Transactions on Sustainable Energy*, vol. 10, no. 2, pp. 853-864, Apr. 2019.

[9] Y. Meng, H. Wang, Z. Duan *et al*., "Small-signal stability analysis and improvement with phase-shift phase-locked loop based on back electromotive force observer for VSC-HVDC in weak grids," *Journal of Modern Power Systems and Clean Energy*, vol. 11, no. 3, pp. 980-989, May 2023.

[10] B. Dasu, S. Mangipudi, and S. Rayapudi, "Small signal stability enhancement of a large scale power system using a bio-inspired whale optimization algorithm," *Protection and Control of Modern Power Systems*, vol. 6, pp. 1-17, Nov. 2021.

[11] S. Bu, W. Du, and H. Wang, "Investigation on probabilistic small-signal stability of power systems as affected by offshore wind generation," *IEEE Transactions on Power Systems*, vol. 30, no. 5, pp. 2479-2486, Sept. 2015.

[12] S. Bu, W. Du, and H. Wang, "Probabilistic analysis of small-signal rotor angle/voltage stability of large-scale AC/DC power systems as affected by grid-connected offshore wind generation," *IEEE Transactions on Power Systems*, vol. 28, no. 4, pp. 3712-3719, Nov. 2013.

[13] V. Gurugubelli, A. Ghosh, and A. K. Panda, "Parallel inverter control using different conventional control methods and an improved virtual oscillator control method in a standalone microgrid," *Protection and Control of Modern Power Systems*, vol. 7, pp. 1-13, Jul. 2022.

[14] P. Li, Y. Wei, J. Qi *et al*., "A closed-form formulation of eigenvalue sensitivity based on matrix calculus for small-signal stability analysis in power system," *Journal of Modern Power Systems and Clean Energy*, vol. 9, no.6, pp. 1436-1445, Nov. 2021.

[15] J. Luo, S. Bu, J. Zhu *et al*., "Modal shift evaluation and optimization for resonance mechanism investigation and mitigation of power systems integrated with FCWG," *IEEE Transactions on Power Systems*, vol. 35, no. 5, pp. 4046-4055, Sept. 2020.

[16] Y. Gu, Y. Li, Y. Zhu *et al*., "Impedance-based whole-system modeling for a composite grid via embedding of frame dynamics," *IEEE Transactions on Power Systems*, vol. 36, no. 1, pp. 336-345, Jan. 2021.

[17] J. Luo, S. Bu, and C. Y. Chung, "Design and comparison of auxiliary resonance controllers for mitigating modal resonance of power systems integrated with wind generation," *IEEE Transactions on Power Systems*, vol. 36, no. 4, pp. 3372-3383, Jul. 2021.

[18] E. J. Routh, *A Treatise on the Stability of a Given State of Motion, Particularly Steady Motion.* London: Macmillan and Company, 1877.

[19] Q. Fu, W. Du, and H. Wang, "Planning of the DC system considering restrictions on the small-signal stability of EV charging stations and comparison between series and parallel connections," *IEEE Transactions on Vehicular Technology*, vol. 69, no. 10, pp. 10724-10735, Oct. 2020.

[20] Y. Zhou, H. Xin, D. Wu *et al*., "Small-signal stability boundary of heterogeneous multi-converter power systems dominated by the phase-locked loops' dynamics," *IEEE Transactions on Energy Conversion*, vol. 37, no. 4, pp. 2874-2888, Dec. 2022.

[21] K. Ji, H. Pang, S. Liu *et al*., "Impedance analysis considering unstable subsystem poles for MMC-HVDC-based wind farm integration system," *CSEE Journal of Power and Energy Systems*, vol. 8, no. 2, pp. 634-639, Mar. 2022.

[22] Y. Xu, Z. Gu, and K. Sun, "Characterization of subsynchronous oscillation with wind farms using describing function and generalized Nyquist criterion," *IEEE Transactions on Power Systems*, vol. 35, no. 4, pp. 2783-2793, Jul. 2020.

[23] L. Fan and Z. Miao, "Admittance-based stability analysis: Bode plots, Nyquist diagrams or eigenvalue analysis?" *IEEE Transactions on Power Systems*, vol. 35, no. 4, pp. 3312-3315, Jul. 2020.

[24] H. Zhang, M. Mehrabankhomartash, M. Saeedifard *et al*., "Stability analysis of a grid-tied interlinking converter system with the hybrid AC/DC admittance model and determinant-based GNC," *IEEE Transactions on Power Delivery*, vol. 37, no. 2, pp. 798-812, Apr. 2022.

[25] M. Y. U. Haque, M. R. Islam, T. Ahmed *et al*., "Improved voltage tracking of autonomous microgrid technology using a combined resonant controller with lead-lag compensator adopting negative imaginary theorem," *Protection and Control of Modern Power Systems*, vol. 7, pp. 1-16, Mar. 2022.

[26] H. Xu, F. Nie, Z. Wang *et al*., "Impedance modeling and stability factor assessment of grid-connected converters based on linear active disturbance rejection control," *Journal of Modern Power Systems and Clean Energy*, vol. 9, no. 6, pp. 1327-1338, Nov. 2021.

[27] A. Arguello, "Setpoint feasibility and stability of wind park control interactions at weak grids," *Journal of Modern Power Systems and Clean Energy*, vol. 10, no. 6, pp. 1790-1796, Nov. 2022.

[28] S. Wu and Z. Liu, "Low-frequency stability analysis of vehicle-grid system with active power filter based on *dq*-frame impedance," *IEEE Transactions on Power Electronics*, vol. 36, no. 8, pp. 9027-9040, Aug. 2021.

[29] S. Wu, Z. Liu, Z. Li *et al*., "Impedance modeling and stability analysis in vehicle-grid system with CHB-STATCOM," *IEEE Transactions on Power Systems*, vol. 35, no. 4, pp. 3026-3039, Jul. 2020.

[30] H. Lin, T. Xue, J. Lyu *et al*., "Impact of different AC voltage control modes of wind-farm-side MMC on stability of MMC-HVDC with offshore wind farms," *Journal of Modern Power Systems and Clean Energy*, vol. 11, no. 4, pp. 1687-1699, Sept. 2023.

[31] L. Harnefors, X. Wang, A. G. Yepes *et al*., "Passivity-based stability assessment of grid-connected VSCs – an overview," *IEEE Journal of Emerging and Selected Topics in Power Electronics*, vol. 4, no. 1, pp. 116-125, Mar. 2016.

[32] C. Chen, W. Du, H. Wang *et al*., "Sub-synchronous oscillations in power systems caused by grid-connected wind farms – a survey of mechanism studies," *CSEE Journal of Power and Energy Systems*, vol. 4, no. 4, pp. 495-503, Dec. 2018.

[33] L. Harnefors, M. Bongiorno, and S. Lundberg, "Input-admittance calculation and shaping for controlled voltage-source converters," *IEEE Transactions on Industrial Electronics*, vol. 54, no. 6, pp. 3323-3334, Dec. 2007.

[34] L. Harnefors, L. Zhang, and M. Bongiorno, "Frequency-domain passivity-based current controller design," *IET Power Electronics*, vol. 1, no. 4, pp. 455-465, Dec. 2008.

[35] G. Wu, Y. He, H. Zhang *et al*., "Passivity-based stability analysis and generic controller design for grid-forming inverter," *IEEE Transactions on Power Electronics*, vol. 38, no. 5, pp. 5832-5843, May 2023.

[36] L. Harnefors, "Proof and application of the positive-net-damping stability criterion," *IEEE Transactions on Power Systems*, vol. 26, no. 1, pp. 481-482, Feb. 2011.

[37] G. Stamatiou and M. Bongiorno, "Stability analysis of two-terminal VSC-HVDC systems using the net-damping criterion," *IEEE Transactions on Power Delivery*, vol. 31, no. 4, pp. 1748-1756, Aug. 2016.

[38] L. Sainz, M. Cheah-Mane, L. Monjo *et al*., "Positive-net-damping stability criterion in grid-connected VSC systems," *IEEE Journal of Emerging and Selected Topics in Power Electronics*, vol. 5, no. 4, pp. 1499-1512, Dec. 2017.

[39] W. Du, B. Ren, H. Wang *et al*., "Comparison of methods to examine sub-synchronous oscillations caused by grid-connected wind turbine generators," *IEEE Transactions on Power Systems*, vol. 34, no. 6, pp. 4931-4943, Nov. 2019.

[40] H. Liu, X. Xie, and W. Liu, "An oscillatory stability criterion based on the unified *dq*-frame impedance network model for power systems with high-penetration renewables," *IEEE Transactions on Power Systems*, vol. 33, no. 3, pp. 3472-3485, May 2018.

[41] X. Xie, Y. Zhan, H. Liu *et al*., "Wide-area monitoring and early-warning of subsynchronous oscillation in power systems with high-penetration of renewables," *International Journal of Electrical Power & Energy Systems*, vol. 108, pp. 31-39, Jun. 2019.

[42] H. Liu, X. Xie, X. Gao *et al*., "Stability analysis of SSR in multiple wind farms connected to series-compensated systems using impedance network model," *IEEE Transactions on Power Systems*, vol. 33, no. 3, pp. 3118-3128, May 2018.

[43] D. Shen, H. Wu, H. Liang *et al*., "Accurate polynomial approximation of bifurcation hypersurfaces in parameter space for small signal stability region considering wind generation," *IEEE Transactions on Power Systems*, vol. 37, no. 6, pp. 4512-4524, Nov. 2022.

[44] L. S. Neves, L. F. C. Alberto, and H. Chiang, "A fast method for detecting limit-induced bifurcation in electric power systems," *Electric Power Systems Research*, vol. 180, Mar. 2020.

[45] C. A. Canizares, N. Mithulananthan, F. Milano *et al*., "Linear performance indices to predict oscillatory stability problems in power systems," *IEEE Transactions on Power Systems*, vol. 19, no. 2, pp. 1104-1114, May 2004.

[46] V. Ajjarapu and B. Lee, "Bifurcation theory and its application to nonlinear dynamical phenomena in an electrical power system," *IEEE Transactions on Power Systems*, vol. 7, no. 1, pp. 424-431, Feb. 1992.

[47] D. Wang, Y. Hou, and J. Hu, "Net damping criterion for stability analysis of grid-tied VSCs in DC voltage control timescale," *CSEE Journal of Power and Energy Systems,* vol. 6, no. 3, pp. 601-609, Sept. 2020.

[48] J. Sun, "Impedance-based stability criterion for grid-connected inverters," *IEEE Transactions on Power Electronics*, vol. 26, no. 11, pp. 3075-3078, Nov. 2011.

[49] X. Wang and F. Blaabjerg, "Harmonic stability in power electronic-based power systems: concept, modeling, and analysis," *IEEE Transactions on Smart Grid*, vol. 10, no. 3, pp. 2858-2870, May 2019.

[50] Y. Liao, Z. Liu, H. Zhang *et al*., "Low-frequency stability analysis of single-phase system with *dq*-frame impedance approach-part II: stability and frequency analysis," *IEEE Transactions on Industry Applications*, vol. 54, no. 5, pp. 5012-5024, Sept.-Oct. 2018.

[51] A. Riccobono and E. Santi, "Comprehensive review of stability criteria for DC power distribution systems," *IEEE Transactions on Industry Applications*, vol. 50, no. 5, pp. 3525-3535, Sept.-Oct. 2014.

[52] N. Hatziargyriou, J. Milanovic, C. Rahmann *et al*., "Definition and classification of power system stability-revisited & extended," *IEEE Transactions on Power Systems*, vol. 36, no. 4, pp. 3271-3281, Jul. 2021.

[53] J. Sun, "Small-signal methods for AC distributed power systems – a review," *IEEE Transactions on Power Electronics,* vol. 24, no. 11, pp. 2545-2554, Nov. 2009.

[54] J. Sun, Z. Bing, and K. J. Karimi, "Input impedance modeling of multipulse rectifiers by harmonic linearization," *IEEE Transactions on Power Electronics*, vol. 24, no. 12, pp. 2812-2820, Dec. 2009.

[55] S. R. Sanders, J. M. Noworolski, X. Liu *et al*., "Generalized averaging method for power conversion circuits," *IEEE Transactions on Power Electronics*, vol. 6, no. 2, pp. 251-259, Apr. 1991.

[56] O. C. Sakinci and J. Beerten, "Generalized dynamic phasor modeling of the MMC for small-signal stability analysis," *IEEE Transactions on Power Delivery*, vol. 34, no. 3, pp. 991-1000, Jun. 2019.

[57] J. Kwon, X. Wang, F. Blaabjerg *et al*., "Harmonic interaction analysis in a grid-connected converter using harmonic state-space (HSS) modeling," *IEEE Transactions on Power Electronics*, vol. 32, no. 9, pp. 6823-6835, Sept. 2017.

[58] M. K. Bakhshizadeh, F. Blaabjerg, J. Hjerrild *et al*., "Improving the impedance-based stability criterion by using the vector fitting method," *IEEE Transactions on Energy Conversion*, vol. 33, no. 4, pp. 1739-1747, Dec. 2018.

[59] W. Zhou, R. E. Torres-Olguin, Y. Wang *et al*., "A gray-box hierarchical oscillatory instability source identification method of multiple-inverter-fed power systems," *IEEE Journal of Emerging and Selected Topics in Power Electronics*, vol. 9, no. 3, pp. 3095-3113, Jun. 2021.

[60] X. F. Wang, Y. Song, M. Irving, *Modern Power Systems Analysis*. New York: Springer, 2010.

[61] W. Du, H. Wang, and S. Bu, *Small-signal Stability Analysis of Power Systems Integrated with Variable Speed Wind Generators*. Cham: Springer, 2018.

[62] S. Bu, X. Zhang, J. B. Zhu *et al*., "Comparison analysis on damping mechanisms of power systems with induction generator based wind power generation," *International Journal of Electrical Power & Energy Systems*, vol. 97, pp. 250-261, Apr. 2018.

[63] C. Zhang, M. Molinas, A. Rygg *et al*., "Impedance-based analysis of interconnected power electronics systems: impedance network modeling and comparative studies of stability criteria," *IEEE Journal of Emerging and Selected Topics in Power Electronics*, vol. 8, no. 3, pp.

2520-2533, Sept. 2020.
[64] Y. Liao, X. Wang, and X. Wang, "Frequency-domain participation analysis for electronic power systems," *IEEE Transactions on Power Electronics*, vol. 37, no. 3, pp. 2531-2537, Mar. 2022.
[65] A. G. J. MacFarlane, "Return-difference and return-ratio matrices and their use in analysis and design of multivariable feedback control systems," *Proceedings of the Institution of Electrical Engineers*, vol. 117, no. 10, pp. 2037-2049, Oct. 1970.
[66] B. Wen, D. Boroyevich, R. Burgos *et al*., "Small-signal stability analysis of three-phase AC systems in the presence of constant power loads based on measured *d-q* frame impedances," *IEEE Transactions on Power Electronics*, vol. 30, no. 10, pp. 5952-5963, Oct. 2015.
[67] D. Yang and Y. Sun, "SISO impedance-based stability analysis for system-level small-signal stability assessment of large-scale power electronics-dominated power systems," *IEEE Transactions on Sustainable Energy*, vol. 13, no. 1, pp. 537-550, Jan. 2022.
[68] J. Hahn, T. Edison, and T. F. Edgar, "A note on stability analysis using Bode plots," *Chemical Engineering Education*, vol. 35, no. 3, pp. 208-211, Jun. 2001.
[69] A. S. Trevisan, A. Mendonca, R. Gagnon *et al*., "Analytically validated SSCI assessment technique for wind parks in series compensated grids," *IEEE Transactions on Power Systems*, vol. 36, no. 1, pp. 39-48, Jan. 2021.
[70] L. Fan and Z. Miao, "Time-domain measurement-based *dq*-frame admittance model identification for inverter-based resources," *IEEE Transactions on Power Systems*, vol. 36, no. 3, pp. 2211-2221, May 2021.
[71] J. Luo, S. Bu, and F. Teng, "An optimal modal coordination strategy based on modal superposition theory to mitigate low frequency oscillation in FCWG penetrated power systems," *International Journal of Electrical Power & Energy Systems*, vol. 120, pp. 1-11, Sept. 2020.
[72] R. D. Middlebrook, "Input filter considerations in design and application of switching regulators," in *Proceedings of IEEE IAS Annual Meeting*, Chicago, USA, Nov. 1976, pp. 366-382.
[73] C. M. Wildrick, F. C. Lee, B. H. Cho *et al*., "A method of defining the load impedance specification for a stable distributed power system," *IEEE Transactions on Power Electronics*, vol. 10, no. 3, pp. 280-285, May 1995.
[74] X. Feng, J. Liu, and F. C. Lee, "Impedance specifications for stable DC distributed power systems," *IEEE Transactions on Power Electronics*, vol. 17, no. 2, pp. 157-162, Mar. 2002.
[75] S. D. Sudhoff, S. F. Glover, P. T. Lamm *et al*., "Admittance space stability analysis of power electronic systems," *IEEE Transactions on Aerospace and Electronic Systems*, vol. 36, no. 3, pp. 965-973, Jul. 2000.
[76] H. G. Kwatny, R. F. Fischl, and C. O. Nwankpa, "Local bifurcation in power systems: theory, computation, and application," *Proceedings of the IEEE*, vol. 83, no. 11, pp. 1456-1483, Nov. 1995.
[77] Y. Gu and T. C. Green, "Power system stability with a high penetration of inverter-based resources," *Proceedings of the IEEE,* vol. 111, no. 7, pp. 832-853, Jul. 2023.
[78] N. Cifuentes, M. Sun, R. Gupta *et al*., "Black-box impedance-based stability assessment of dynamic interactions between converters and grid," *IEEE Transactions on Power Systems*, vol. 37, no. 4, pp. 2976-2987, Jul. 2022.
[79] G. Gaba, S. Lefebvre, and D. Mukhedkar, "Comparative analysis and study of the dynamic stability of AC/DC systems," *IEEE Transactions on Power Systems*, vol. 3, no. 3, pp. 978-985, Aug. 1988.
[80] C. Li, Y. Chen, T. Ding *et al*., "A sparse and low-order implementation for discretization-based eigen-analysis of power systems with time-delays," *IEEE Transactions on Power Systems*, vol. 34, no. 6, pp. 5091-5094, Nov. 2019.
[81] P. De Rua, Ö. C. Sakinci, and J. Beerten, "Comparative study of dynamic phasor and harmonic state-space modeling for small-signal stability analysis," *Electric Power Systems Research*, vol. 189, p. 106626, Dec. 2020.
[82] A. Ramirez, "Vector fitting-based calculation of frequency-dependent network equivalents by frequency partitioning and model-order reduction," *IEEE Transactions on Power Delivery*, vol. 24, no. 1, pp. 410-415, Jan. 2009.
[83] Y. Liao and X. Wang, "Impedance-based stability analysis for interconnected converter systems with open-loop RHP poles," *IEEE Transactions on Power Electronics*, vol. 35, no. 4, pp. 4388-4397, Apr. 2020.
[84] F. Liu, J. Liu, H. Zhang *et al*., "Stability issues of Z+Z type cascade system in hybrid energy storage system (HESS)," *IEEE Transactions on Power Electronics*, vol. 29, no. 11, pp. 5846-5859, Nov. 2014.

Qifan Chen received the B.Eng. and M.Eng. degrees in electrical engineering from Fuzhou University, Fuzhou, China, in 2018 and 2021, respectively. He is currently working toward the Ph.D. degree with the Department of Electrical and Electronic Engineering, The Hong Kong Polytechnic University, Hong Kong, China. His research interests include power system transient stability and small-signal stability analysis, and the application of machine learning in power system stability.

Siqi Bu received the Ph.D. degree from the electric power and energy research cluster, The Queen's University of Belfast, Belfast, U.K., where he continued his postdoctoral research work before entering industry. Then, he was with National Grid UK as an experienced UK National Transmission System Planner and Operator. He is an Associate Professor and Associate Head with Department of Electrical and Electronic Engineering, The Hong Kong Polytechnic University, Hong Kong, China, and also a Chartered Engineer with UK Royal Engineering Council, London, U.K. His research interests include power system stability analysis and operation control, considering renewable energy integration, and smart grid application.

Chi Yung Chung received the B.Eng. (Hons.) and Ph.D. degrees in electrical engineering from The Hong Kong Polytechnic University, Hong Kong, China, in 1995 and 1999, respectively. He is currently the Head and the Chair Professor of Power Systems Engineering with the Department of Electrical and Electronic Engineering, The Hong Kong Polytechnic University. He is an IEEE PES Distinguished Lecturer. He was a recipient of the 2021 IEEE Canada P. Ziogas Electric Power Award. He is a Senior Editor of IEEE Transactions on Power Systems, a Consulting Editor of IEEE Transactions on Sustainable Energy, and the Vice Editor-in-Chief of Journal of Modern Power Systems and Clean Energy. His current research interests include smart grid technologies, renewable energy, power system stability/control, planning and operation, computational intelligence applications, power markets, and electric vehicle charging.